DECLASSIFIED
CONFIDENTIAL

393

Copy
RM L55K16

NACA RM L55K16

GROUP (4)
DOWNGRADED AT 3 YEAR INTERVALS; DECLASSIFIED AFTER 12 YEARS.

NACA

RESEARCH MEMORANDUM

Declassified by authority of NASA
Classification Change Notices No. 213
Dated ** JUN 30 1971

FLIGHT INVESTIGATION AT LOW ANGLES OF ATTACK TO DETERMINE THE LONGITUDINAL STABILITY AND CONTROL CHARACTERISTICS OF A CRUCIFORM CANARD MISSILE CONFIGURATION WITH A LOW-ASPECT-RATIO WING AND BLUNT NOSE AT MACH NUMBERS FROM 1.2 TO 2.1

By Clarence A. Brown, Jr.

Langley Aeronautical Laboratory
Langley Field, Va.

CLASSIFICATION CHANGED
TO UNCLASSIFIED
By Authority of TD-70180 Date 1 MAR 1971

CLASSIFIED DOCUMENT

This material contains information affecting the National Defense of the United States within the meaning of the espionage laws, Title 18, U.S.C., Secs. 793 and 794, the transmission or revelation of which in any manner to an unauthorized person is prohibited by law.

NATIONAL ADVISORY COMMITTEE
FOR AERONAUTICS

WASHINGTON

September 30, 1957

CATEGORY
SPECIAL HANDLING

CONFIDENTIAL

DECLASSIFIED
CONFIDENTIAL

NATIONAL ADVISORY COMMITTEE FOR AERONAUTICS

RESEARCH MEMORANDUM

FLIGHT INVESTIGATION AT LOW ANGLES OF ATTACK TO DETERMINE THE LONGITUDINAL STABILITY AND CONTROL CHARACTERISTICS OF A CRUCIFORM CANARD MISSILE CONFIGURATION WITH A LOW-ASPECT-RATIO WING AND BLUNT NOSE AT MACH NUMBERS FROM 1.2 TO 2.1[1]

By Clarence A. Brown, Jr.

SUMMARY

A full-scale rocket-powered model of a cruciform canard missile configuration with a low-aspect-ratio wing and blunt nose has been flight tested by the Langley Pilotless Aircraft Research Division. Static and dynamic longitudinal stability and control derivatives of this interdigitated canard-wing missile configuration were determined by using the pulsed-control technique at low angles of attack and for a Mach number range of 1.2 to 2.1.

The lift-curve slope showed only small nonlinearities with changes in control deflection or angle of attack but indicated a difference in lift-curve slope of approximately 7 percent for the two control deflections of $\delta \approx 3.0^{\circ}$ and $\delta \approx -0.3^{\circ}$. The large tail length of the missile tested was effective in producing damping in pitch throughout the Mach number range tested. The aerodynamic-center location was nearly constant with Mach number for the two control deflections but was shown to be less stable with the larger control deflection. The increment of lift produced by the controls was small and positive throughout the Mach number range tested, whereas the pitching moment produced by the controls exhibited a normal trend of reduced effectiveness with increasing Mach number. The effectiveness of the controls in producing angle of attack, lift, and pitching moment was good at all Mach numbers tested.

[1]The information presented herein was previously given limited distribution.

CONFIDENTIAL

INTRODUCTION

The Langley Pilotless Aircraft Research Division has initiated a program to investigate the general aerodynamic characteristics of a full-scale rocket-powered cruciform canard missile configuration with a low-aspect-ratio wing and blunt nose. This paper presents the results from a flight test investigation using the pulsed-control technique to determine the static and dynamic longitudinal stability and control derivatives and drag data for a canard-missile configuration. The methods for obtaining these data are presented in references 1 and 2. This investigation was conducted at a small angle-of-attack range and for a Mach number range of 1.2 to 2.1. The model used in this investigation was flight-tested at the Langley Pilotless Aircraft Research Station at Wallops Island, Va.

SYMBOLS

S_w	total wing area in one plane including body intercept, sq ft
S_e	exposed canard area in one plane, sq ft
$\bar{c}$	wing mean aerodynamic chord, ft
S_b	body cross-sectional area, sq ft
d	body diameter, ft
W	model weight, lb
I_y	moment of inertia about Y-axis, slug-ft^2
I_x	moment of inertia about X-axis, slug-ft^2
R	Reynolds number
M	Mach number
g	acceleration due to gravity, ft/sec^2
q	dynamic pressure, lb/ft^2

DECLASSIFIED

b exponential damping constant, e^{-bt}, per second

P period of oscillation, sec

$\beta = \sqrt{M^2 - 1}$

A aspect ratio

α angle of attack, deg

α_{trim} trim angle of attack, deg

$\dot{\alpha}$ $\frac{1}{57.3}\frac{d\alpha}{dt}$, radians/sec

δ control deflection, deg

$\dot{\theta}$ pitching velocity, radians/sec

A_n/g normal accelerometer reading, g units

A_l/g longitudinal accelerometer reading, g units

A_t/g transverse accelerometer reading, g units

C_D drag coefficient, $\left(-A_l/g \cos \alpha + A_n/g \sin \alpha\right)\frac{W}{qS_b}$

C_L lift coefficient, $\left(A_n/g \cos \alpha + A_l/g \sin \alpha\right)\frac{W}{qS_b}$

C_m pitching-moment coefficient, $\frac{\text{Pitching moment about center of gravity}}{qS_b d}$

$\frac{\Delta C_L}{\Delta \delta}$ average lift coefficient per unit control deflection

$\frac{\Delta C_m}{\Delta \delta}$ average pitching-moment coefficient per unit control deflection

C_N normal-force coefficient, $A_n/g \frac{W}{qS_b}$

C_Y lateral-force coefficient, $A_t/g \frac{W}{qS_b}$

C_R resultant-force coefficient corrected for trim, $\left[\left(C_N - C_{N_{trim}}\right)^2 + \left(C_Y - C_{Y_{trim}}\right)^2\right]^{1/2}$

Derivatives:

$C_{L_\alpha} = \frac{\partial C_L}{\partial \alpha}$, per degree

$C_{m_\alpha} = \frac{\partial C_m}{\partial \alpha}$, per degree

$C_{m_\delta} = \frac{\partial C_m}{\partial \delta}$, per degree

$C_{m_q} = \frac{\partial C_m}{\partial \left(\frac{\dot{\theta} d}{2V}\right)}$, per radian

$C_{m_{\dot{\alpha}}} = \frac{\partial C_m}{\partial \left(\frac{\dot{\alpha} d}{2V}\right)}$, per radian

MODEL AND APPARATUS

Model Description

Sketches of the rocket-powered model used in this test are shown in figure 1. Sketches of the canard surface and wing surface are shown in figure 2. Photographs of the model and model booster combination are shown in figures 3 and 4. Physical characteristics determined by preflight measurements are presented in table I.

The body of the model had a maximum diameter of 5 inches with a fineness ratio of 22.95. The nose section consisted of a 2.6-inch-radius spherical segment that was faired into the 5-inch-diameter body. Protruding in front of the spherical nose section was a sting used to mount part of the instrumentation of the model (figs. 1 and 3). The canard surfaces were of arrow wing plan form with a modified hexagonal airfoil section having a maximum thickness at the wing-body juncture of 3.3 percent (fig. 2). The leading edges of the canard surfaces were swept back 66° 34' and the trailing edges were swept back 14° 31' (fig. 2). The canard surfaces were pivoted about a hinge line located at 46 percent of the mean geometric chord.

The wings were interdigitated 45° to the canard surfaces and were of trapezoidal plan form with the leading edge swept back 45° (fig. 2). The wing had a modified hexagonal airfoil section with a constant thickness corresponding to a thickness ratio of 1.2 percent at the wing-body juncture.

The control surfaces were actuated by a slow-acting solid-propellant gas-driven servo explained in reference 3. In order to use the gas-driven servo to disturb the model in pitch abruptly, it was necessary to reduce the rise time of the control surfaces. Static firing of the pulse unit, prior to flight test of the model and at the desired control deflection range, resulted in changes that reduced the rise time to approximately 0.06 second. The length of time for a fixed control deflection was approximately 0.6 second throughout the flight of the model. The solid propellant used in the gas-driven servo was capable of operating the pulse mechanism for approximately 10 seconds.

Instrumentation

The model was equipped with an NACA nine-channel telemeter which transmitted a continuous record of normal (two locations), transverse and longitudinal accelerations, angle of attack, angle of sideslip, control deflection, total pressure, and static pressure. The transverse, longitudinal, and one normal accelerometer were located so as to be on the center of gravity of the model when the sustainer motor had burned out; and a second normal accelerometer was mounted on the model center line and 45 inches ahead of the center of gravity of the model. Angle of attack and angle of sideslip were measured by a free-floating vane mounted on a sting which protruded from the nose of the model. Total pressure was obtained by a total-pressure tube extended from the fuselage ahead of the wings and in a plane $22\frac{1}{2}^{\circ}$ to the main wing and canard surfaces. A static-pressure orifice was located on the cylindrical section of the fuselage ahead of the canard surfaces. Approximate values of rate of roll were obtained by NACA spinsonde equipment in conjunction with the telemeter antenna which was plane polarized.

Model velocity was obtained from the CW Doppler radar unit and the model trajectory was determined through use of an NACA modified SCR-584 radar tracking unit. A radiosonde, released at the time of flight, was used to obtain atmospheric data throughout the altitude range traversed by the model.

TEST TECHNIQUE

The model was launched at an elevation angle of approximately 45° from a zero-length launcher as shown in figure 4. The model was boosted to supersonic velocity by two 6-inch-diameter solid-propellant rocket motors which together delivered approximately 12,000 pounds of thrust for 3.0 seconds. After separation from the booster, a sustainer motor, made as an integral part of the model, delivered approximately 2,500 pounds of thrust for 2.6 seconds and propelled the model to the peak Mach number

of 2.47. After the sustainer burnout, the model was disturbed in pitch by a programed square-wave deflection of the canard surfaces. Transient responses to the step input of the control surface were continuously recorded in the form of time histories as the model decelerated through the Mach number range.

The canard control surfaces in the horizontal plane were pulsed in a square-wave motion by deflecting them abruptly to a $\delta \approx 3.0^\circ$ and holding them in that position for a predetermined time interval of approximately 0.6 second, then deflecting them again abruptly to a $\delta \approx -0.3^\circ$ and holding them again at this deflection for the same time interval. This sequence was repeated throughout the flight of the model. The canard control surfaces of the vertical plane were locked in the zero position and remained in that position throughout the flight of the model.

PRECISION OF DATA

Correction

The velocity data, as obtained by the CW Doppler velocimeter, were corrected for flight-path curvature and wind effects at altitude. The magnitudes and direction of these winds were determined by tracking the radiosonde balloon.

In order to obtain the angle of attack at the center of gravity of the model, the angle of attack measured at the nose was corrected for model pitching velocity by the method presented in reference 4.

Accuracy

The maximum possible errors in accuracy of the quantities listed below, on the basis of the accuracies of the instrumentation and dynamic pressure are presented for two Mach numbers:

M	Limit of accuracy of —					
	M	α	δ	C_L	C_m	$C_{D_{min}}$
1.30	±0.01	±0.50	±0.20	±0.17	±0.60	±0.08
2.00	±0.02	±0.50	±0.20	±0.06	±0.16	±0.05

DECLASSIFIED

It should be pointed out that the quantities listed in the table on the preceding page are based on body cross-sectional area. From a consideration of previous experience, probable errors are 50 percent less that those just quoted. Parameters dependent upon differences in measured quantities or slopes such as C_{l_α} are much more accurately determined than the previously mentioned errors would indicate.

RESULTS AND DISCUSSION

Complete data were received for the model tested for a Mach number range of 1.2 to 2.1. The Reynolds number of this test ranged from approximately 4.7×10^6 to 10.7×10^6, per foot. Variation of Reynolds number with Mach number for this test is shown in figure 5.

Lift Coefficient

Shown in figure 6 are plots of lift coefficient against angle of attack for the two control deflections of $\delta \approx -0.3^\circ$ and $\delta \approx 3.0^\circ$. These plots are typical lift coefficient against angle-of-attack plots for this model. In order to present lift coefficient against angle of attack and retain clarity, only one increasing and decreasing angle of attack for each disturbance is presented. The hysteresis noted in the data is not unusual for a canard-type configuration. Several other pulsed control models have also experienced this hysteresis characteristic (refs. 1, 2, and 5), and the effect upon the lift-curve slope is negligible. Presented in figure 7 are the lift-curve slopes against Mach number from figure 6 and for similar plots at other Mach numbers. The lift-curve slope showed only small nonlinearities with changes in control deflection or angle of attack but indicated a difference in lift-curve slope of approximately 7 percent for the two control deflections of $\delta \approx 3.0^\circ$ and $\delta \approx -0.3^\circ$. As would be expected, the lift-curve slope exhibited a smooth variation with Mach number throughout the Mach number range tested.

Also presented in figure 7 is a theoretical lift-curve slope calculated from reference 6. Agreement between the theoretical and measured lift-curve slopes below a Mach number of 1.60 is poor. Some of this disagreement might be explained in that for the configuration tested the low aspect ratio of the rearward surfaces and reduced Mach numbers decreased the effective wing aspect ratio (βA) to a value less than one. When the effective aspect ratio is less than one, the basic theoretical lift curve as determined by the linear theory of reference 6 was beyond the scope of the theory and necessitated using a theoretical

lift-curve slope which the authors of reference 6 found necessary to extrapolate. Above a Mach number of 1.60 the agreement between the measured lift-curve slope and the theoretical values varied from 4 to 15 percent.

Dynamic Stability

The exponential damping constant b is presented in figure 8 for the two control deflections. The damping-in-pitch derivative $C_{m_q} + C_{m_{\dot{\alpha}}}$ obtained from the faired curve of b is presented in figure 9. The damping-in-pitch derivative $C_{m_q} + C_{m_{\dot{\alpha}}}$ increased from -7,000 at a Mach number of 1.24 to -11,820 at a Mach number of 1.55, then decreased gradually to a value of -8,600 at a Mach number of 2.13. As a result of the model roll rate being between 0 and 3 radians per second, it was necessary to analyze the resultant-force coefficient time history of the normal and transverse motion by the method presented in reference 2 to obtain the damping of the model.

The damping-in-pitch derivative $C_{m_q} + C_{m_{\dot{\alpha}}}$ for the model of the present test compares favorably with the damping of the model of reference 5 and, as might be expected, the large tail length of the present model was effective in producing damping in pitch for the Mach number range tested.

Static Stability

The longitudinal period of oscillation of the model using the resultant force time histories is presented in figure 10 as a function of Mach number.

Two methods were used in obtaining the pitching-moment derivative C_{m_α} presented in figure 11. The faired curve of C_{m_α} was reduced from the faired curve of period of oscillation of the model. The plotted points of figure 11 were obtained by taking the slopes of pitching moment against angle of attack. Plots of the pitching moment against angle of attack are presented in figure 12 for the two control deflections of $\delta \approx -0.3^\circ$ and $\delta \approx 3.0^\circ$. The total pitching moment was obtained by the use of the two normal accelerometers, one located at the model center of gravity and the other located 45 inches ahead of the model center of gravity. The part of the pitching moment due to the angle of attack can then be obtained by subtracting that part which was contributed by the model damping. As may be seen in figure 12 some hysteresis is noticeable for most of the control deflections and

DECLASSIFIED

examination of these curves reveals only slight nonlinearities. Comparison of these slopes and the pitching-moment derivative obtained from the period of oscillation (fig. 11) indicates good agreement between the two methods of obtaining this derivative.

Aeordynamic-center location was determined from the C_{m_α} curve and the faired C_{L_α} curves and is presented in figure 13 in terms of inches from station 0 against Mach number. The two curves for the aerodynamic-center position resulted from the two values of C_{L_α} for the two control deflections. The aerodynamic center was nearly constant with Mach number for either control deflection but was shown to be slightly less stable with $\delta \approx 3.0^\circ$ than with $\delta \approx -0.3^\circ$.

Also included in figure 13 are the loaded and empty center-of-gravity locations in station numbers and a theoretical aerodynamic-center location from reference 6. As mentioned previously, some of the disagreement between the experimental and theoretical values is due to using a theoretical lift-curve slope determined by the linear theory of reference 6. The theoretical lift-curve slope of figure 13 was beyond the scope of the theory of reference 6 and, as a result, it was necessary to use a theoretical lift-curve slope which the authors of reference 6 determined by extrapolation.

Control Effectiveness

The trim angles of attack are shown in figure 14 as a function of Mach number for the two control deflections of $\delta \approx 3.0^\circ$ and $\delta \approx -0.3^\circ$. It was expected that, for the symmetrical model tested, the model would trim at $\alpha = 0^\circ$ for $\delta = 0^\circ$. The apparent out of trim shown in figure 14 may have resulted from indicator out of trim or asymmetries due to model construction.

The ratio of the trim angle of attack to the trim control deflection for the model tested is presented in figure 15. The effectiveness of the controls in producing angle of attack can be seen in figure 15 to decrease slightly with increasing Mach number until $M = 1.60$ and then to increase gradually with increasing Mach number. It should be noted that the effectiveness of the controls in producing angle of attack is as good at low supersonic Mach numbers ($M = 1.3$) as at the higher supersonic Mach numbers ($M = 2.1$).

The control derivatives $\frac{\Delta C_L}{\Delta \delta}$ and $\frac{\Delta C_m}{\Delta \delta}$ of the model tested are presented in figures 16 and 17, respectively. Figure 16 shows that the increment of lift due to the canard deflection $\frac{\Delta C_L}{\Delta \delta}$ is small and

positive at all Mach numbers tested. The fact that $\frac{\Delta C_L}{\Delta \delta}$ is positive means that the lift of the control surface itself exceeds the loss of lift on the wing due to downwash of the canards. This condition can probably be attributed to the interdigitation of the wings and canards reducing the downwash at the small angles of attack of the test and to the size of the canards themselves. Presented also in figure 16 is a plot of C_{L_δ} as obtained from reference 6. Both reference 6 and the test $\frac{\Delta C_L}{\Delta \delta}$ indicated positive values throughout the Mach number range tested.

Pitching effectiveness of the canard-control surface of the model (fig. 17) was positive through the Mach number range tested and decreased from 1.56 at a Mach number of 1.30 to a value of 1.08 at a Mach number of 2.10, a normal trend of reduced effectiveness with increasing Mach number being exhibited.

For the large static margin of the test, 16 to 21 inches, the effectiveness of the controls in producing angle of attack, lift, and pitching moment is good. Since this particular configuration will fly near trim conditions at all times, control surfaces such as these will give good maneuverability and still remain near trim conditions. If greater maneuverability is desired, however, it is possible to reduce the static margin approximately 7 inches and still retain a stable configuration at low supersonic Mach numbers and loaded conditions.

Drag

Drag data for the model tested are presented in the form of $C_{D_{min}}$, based on fuselage cross-sectional area, against Mach number in figure 18. The minimum drag coefficient varied smoothly with Mach number from 1.48 at a Mach number of 1.15 to 1.20 at a Mach number of 2.20.

Also presented in figure 18 are the zero-lift drag coefficient against Mach number for two other missile configurations (unpublished data) and the $C_{D_{min}}$ for the model tested. Models A and B, taken from unpublished data, were similar to the model tested, several changes being made to the models that affect the drag coefficient. These changes were as follows:

1. Models A and B did not have an angle-of-attack, angle-of-sideslip indicator.

2. Models A and B were approximately 8 inches shorter.

3. Models A and B were roll-rate stabilized with air-driven gyro-actuated rollerons. Model A experienced a high-frequency roll instability in flight which caused the rollerons to deflect violently at the same

DECLASSIFIED

frequency as the roll instability. This roll instability was eliminated in model B without changing the exterior parts of the model. Although model A experienced a high-frequency roll instability, the roll-rate stabilization system did roll-rate stabilize the model within a roll rate of $\pm 20^{\circ}$ per second. Comparison of the drag coefficients of model A and model B shows that elimination of the roll instability and thereby elimination of the violent deflection of the rollerons resulted in a reduction of drag coefficient of approximately 8 to 40 percent at Mach numbers of 1.95 and 1.25, respectively.

As previously mentioned, the model used in this investigation did not have a roll-rate stabilization system as did models A and B but an angle-of-attack, angle-of-sideslip indicator protruded from the nose of the model. The drag coefficients of the present model and model B differed from approximately 20 percent to 40 percent at Mach numbers of 1.15 and 2.18, respectively. This reduction of drag coefficient can be attributed in part to the elimination of the roll-rate stabilization system and the angle-of-attack, angle-of-sideslip indicator acting as a windshield or spike. Experimental results have shown that drag reductions to spherical nose sections can be made by the use of spikes or windshields. For example, reference 7 shows that the addition of a spike to a spherical nose will reduce the drag of the model from 15 percent at a Mach number of 1.30 to 40 percent at a Mach number of 1.60.

CONCLUSIONS

The results of a flight test of the full-scale rocket-powered cruciform canard missile configuration for a Mach number range of 1.23 to 2.1 indicated the following conclusions:

1. The lift-curve slope showed only small nonlinearities with changes in control deflection or angle of attack but indicated a difference in lift-curve slope of approximately 7 percent for the two control deflections of $\delta \approx 3.0^{\circ}$ and $\delta \approx -0.3^{\circ}$.

2. The large tail length of the model was effective in producing damping in pitch throughout the Mach number range tested.

3. The aerodynamic-center location was nearly constant with Mach number for either control deflection but was shown to be slightly less stable with the larger control deflection.

4. The increment of lift produced by the controls $\frac{\Delta C_L}{\Delta \delta}$ was small and positive throughout the Mach number range.

5. The effectiveness of the controls in producing pitching moment $\frac{\Delta C_m}{\Delta \delta}$ exhibited a normal trend of reduced effectiveness with increased Mach number.

Langley Aeronautical Laboratory,
National Advisory Committee for Aeronautics,
Langley Field, Va., November 2, 1955.

DECLASSIFIED

REFERENCES

1. Niewald, Roy J., and Moul, Martin T.: The Longitudinal Stability, Control Effectiveness, and Control Hinge-Moment Characteristics Obtained From a Flight Investigation of a Canard Missile Configuration at Transonic and Supersonic Speeds. NACA RM L50I27, 1950.

2. Baber, Hal T., Jr., and Moul, Martin T.: Longitudinal Stability and Control Characteristics As Determined by the Rocket-Model Technique for an Inline, Cruciform, Canard Missile Configuration With a Low-Aspect-Ratio Wing Having Trailing-Edge Flap Controls for a Mach Number Range of 0.7 to 1.8. NACA RM L54B12, 1955.

3. Blaise, Robert A.: Report of Flight Tests of SIDEWINDER (EX-0) Missiles 1X, 2X, 3X, and 4X. NOTS TM 273, U. S. Naval Ord. Test Station (Inyokern, Calif.), Oct. 10, 1952.

4. Ikard, Wallace L.: An Air-Flow-Direction Pickup Suitable for Telemetering Use on Pilotless Aircraft. NACA TN 3799, 1956. (Supersedes NACA RM L53K16.)

5. Brown, Clarence A., Jr., and Lundstrom, Reginald R.: Flight Investigation From Mach Number 0.8 to Mach Number 2.0 To Determine Some Effects of Wing-to-Tail Distance on the Longitudinal Stability and Control Characteristics of a 60° Delta-Wing—Canard Missile. NACA RM L52C26, 1952.

6. Nielsen, Jack N., Kaattari, George E., and Anastasio, Robert F.: A Method for Calculating the Lift and Center of Pressure of Wing-Body-Tail Combinations at Subsonic, Transonic, and Supersonic Speeds. NACA RM A53G08, 1953.

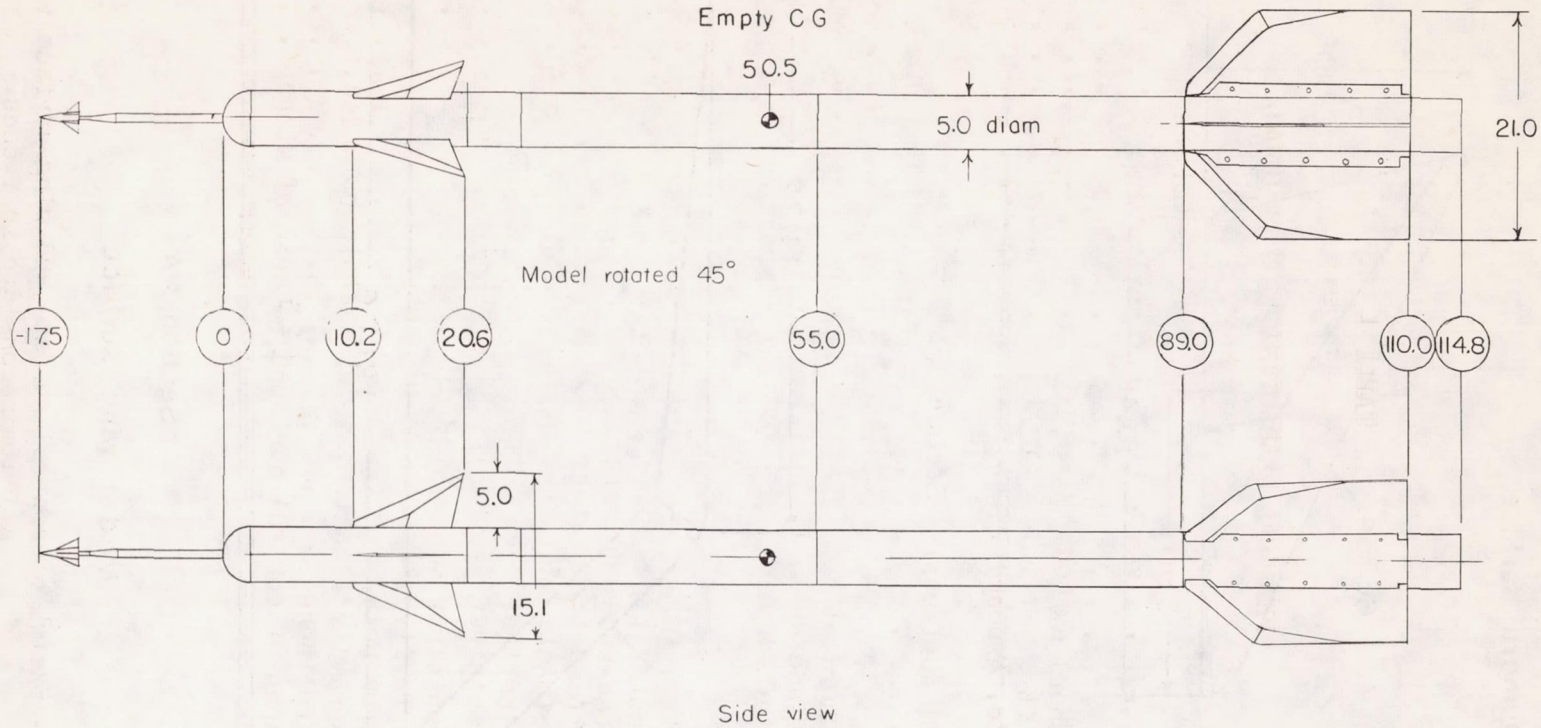
7. Piland, Robert O.: Preliminary Free-Flight Investigation of the Zero-Lift Drag Penalities of Several Missile Nose Shapes for Infrared Seeking Devices. NACA RM L52F23, 1952.

TABLE I

PHYSICAL CHARACTERISTICS OF MODEL

Wing:	
S_w, sq ft	2.839
$\bar{c}$, ft	1.650
Thickness/Chord at body juncture	0.012
Wing span, ft	1.750
Aspect ratio, exposed	0.834
Canard control surfaces:	
S_e, sq ft	0.358
$\bar{c}$, ft	0.651
Thickness/Chord at body juncture	0.033
Control-surface span, ft	1.260
Aspect ratio, exposed	1.980
General:	
Body diameter, in.	5.000
Fineness ratio	22.95
A, body cross-sectional area, sq ft	0.136
Weight, lb (model sustainer loaded)	158.25
Weight, lb (model sustainer empty)	121.25
Moment of inertia:	
Model, sustainer empty, I_y, slug-ft^2	37.52
Model, sustainer empty, I_x, slug-ft^2	0.215
Center-of-gravity location, model sustainer empty, inches from nose	50.50
Center-of-gravity location, model sustainer loaded, inches from nose	58.00
Ratio of span of control surfaces to span of wings	0.72

CONFIDENTIAL



Side view

Figure 1.- Sketch of model tested. All dimensions are in inches.

CONFIDENTIAL

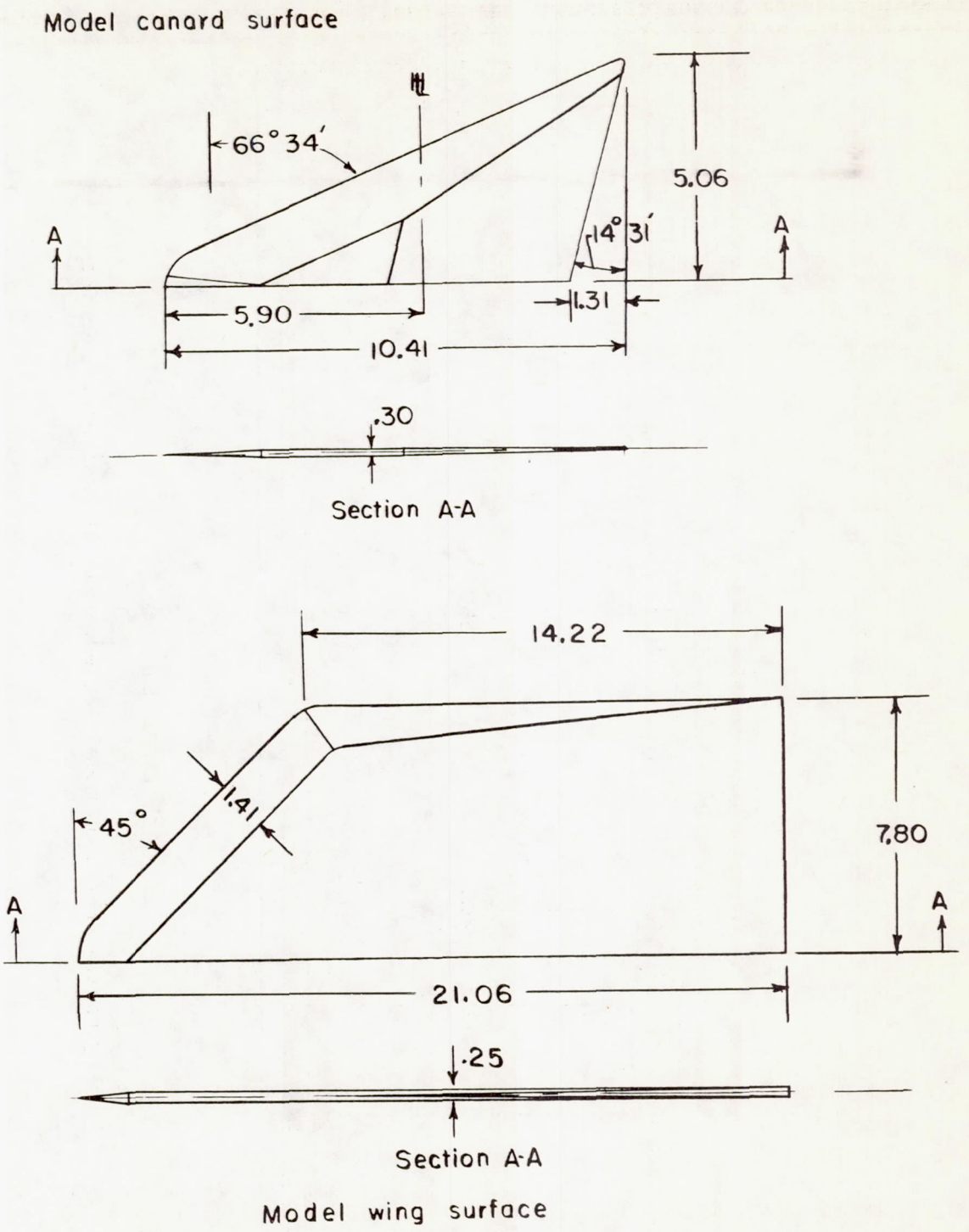
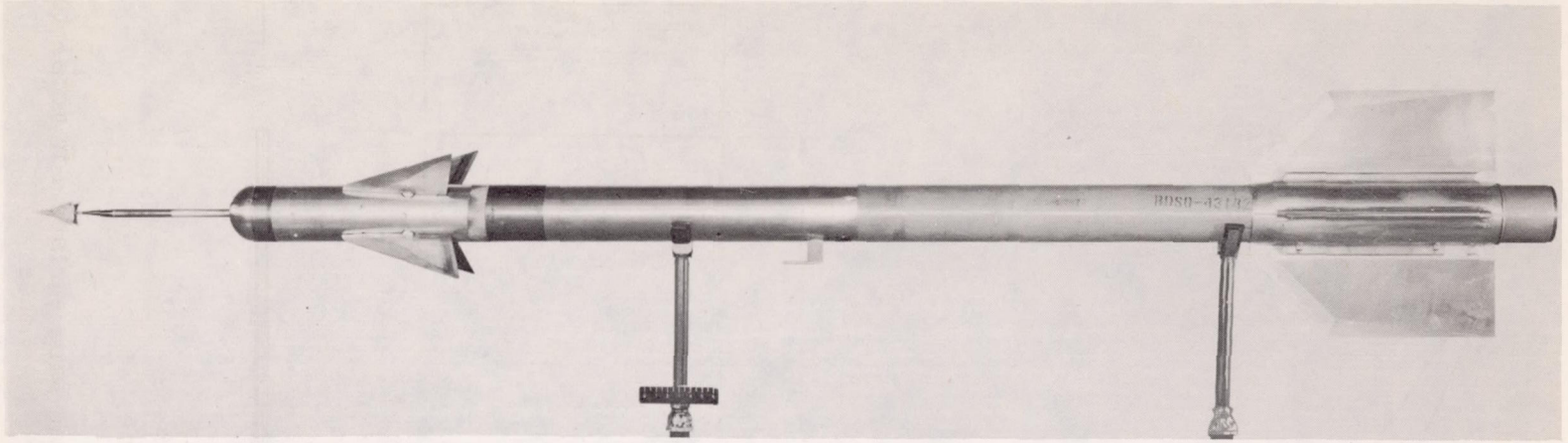
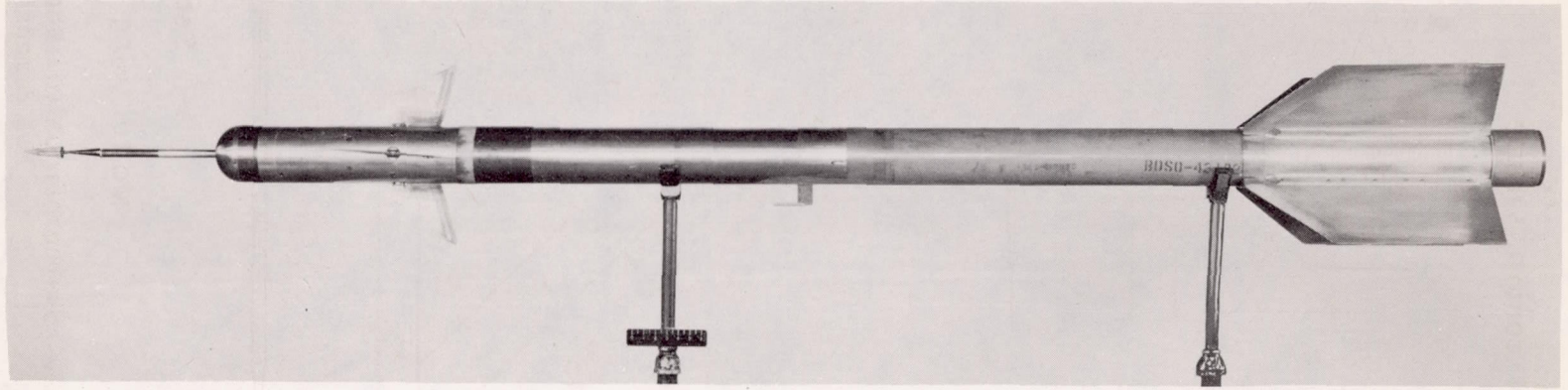


Figure 2.- Sketch of control surface and wing surface for model tested. All dimensions are in inches.

CONFIDENTIAL



Model rotated 45°

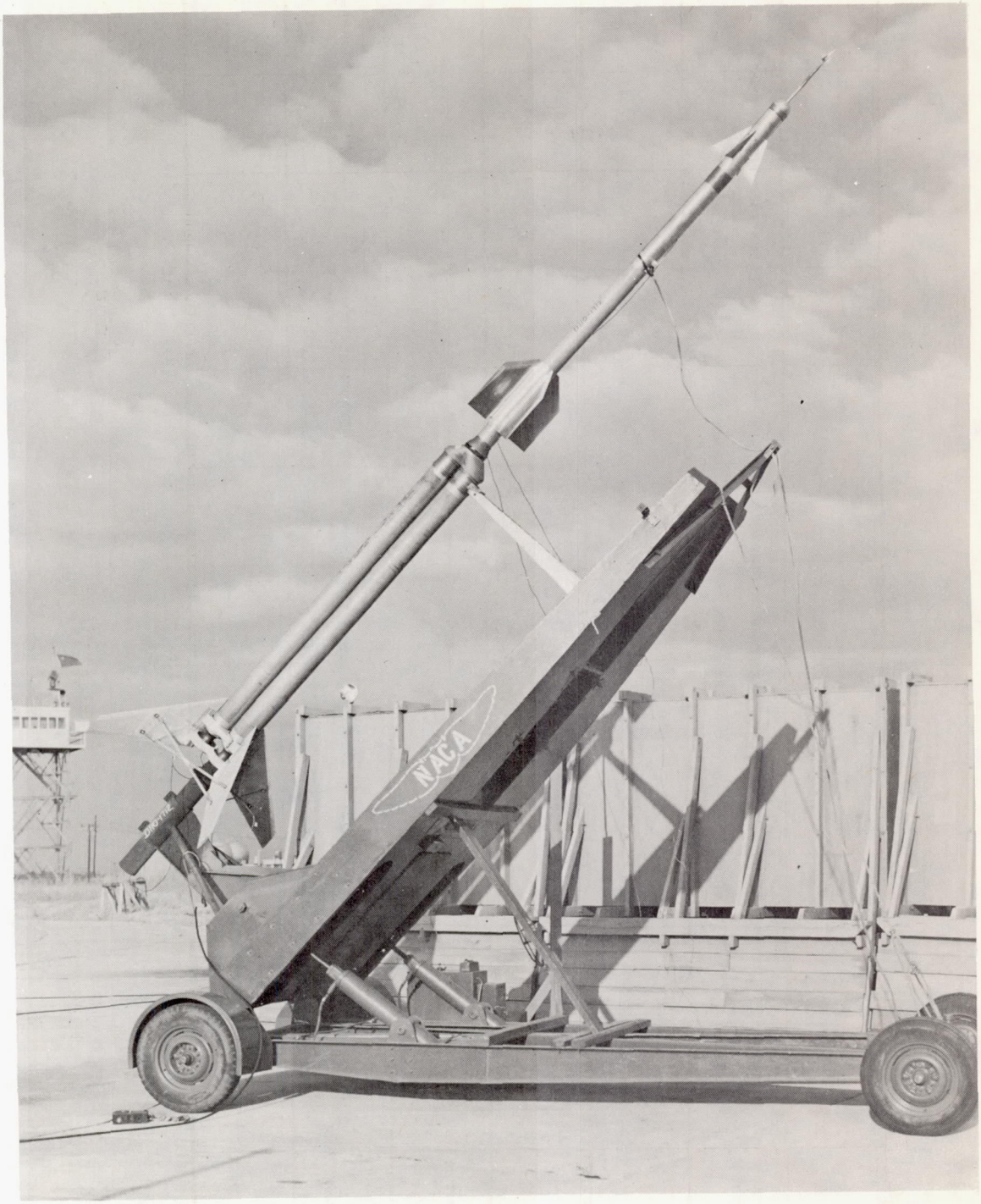


Side view

L-90562

Figure 3.- Photographs of model tested.

CONFIDENTIAL



L-87727

Figure 4.- Photograph of model and booster prior to launching.

CONFIDENTIAL

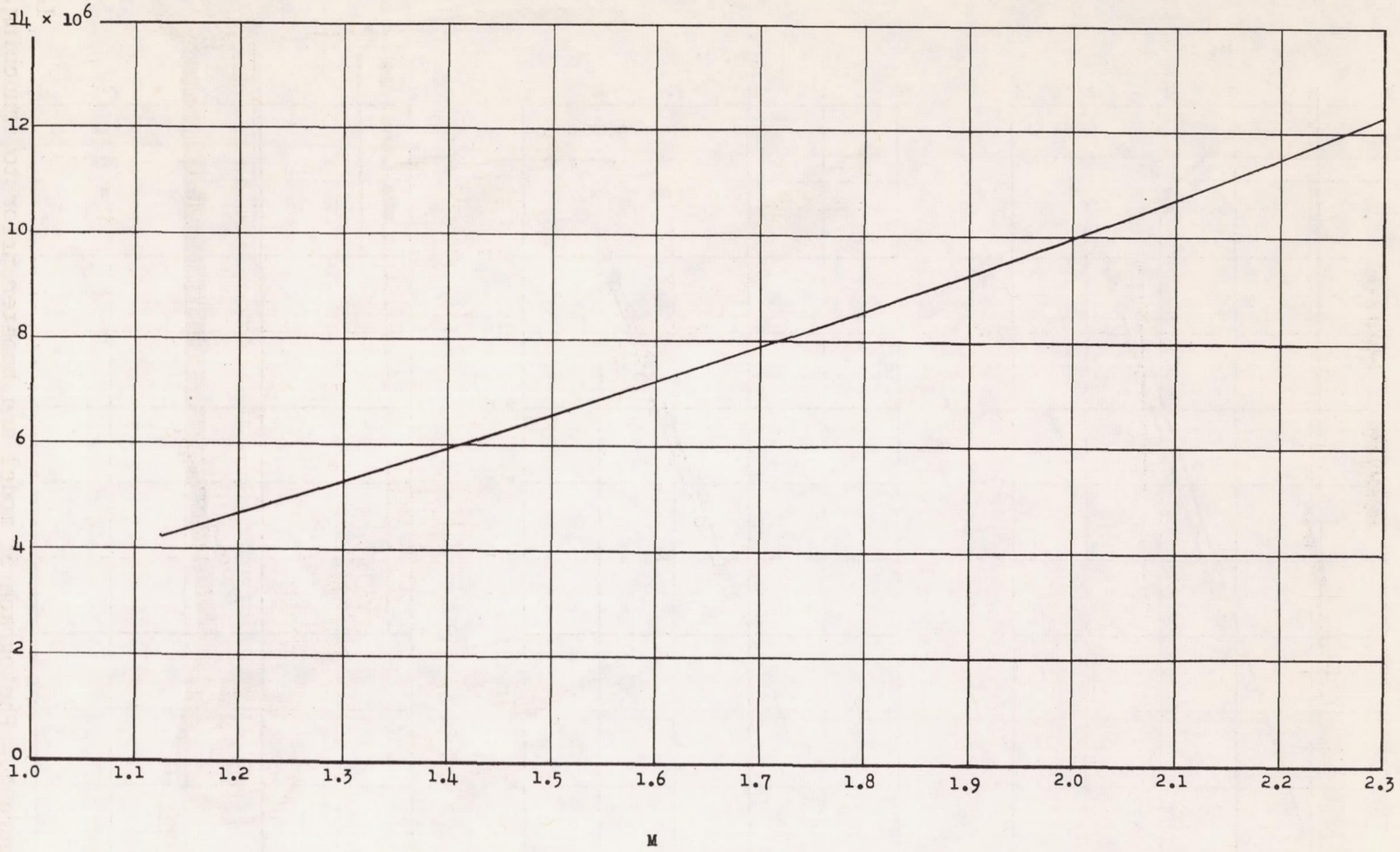
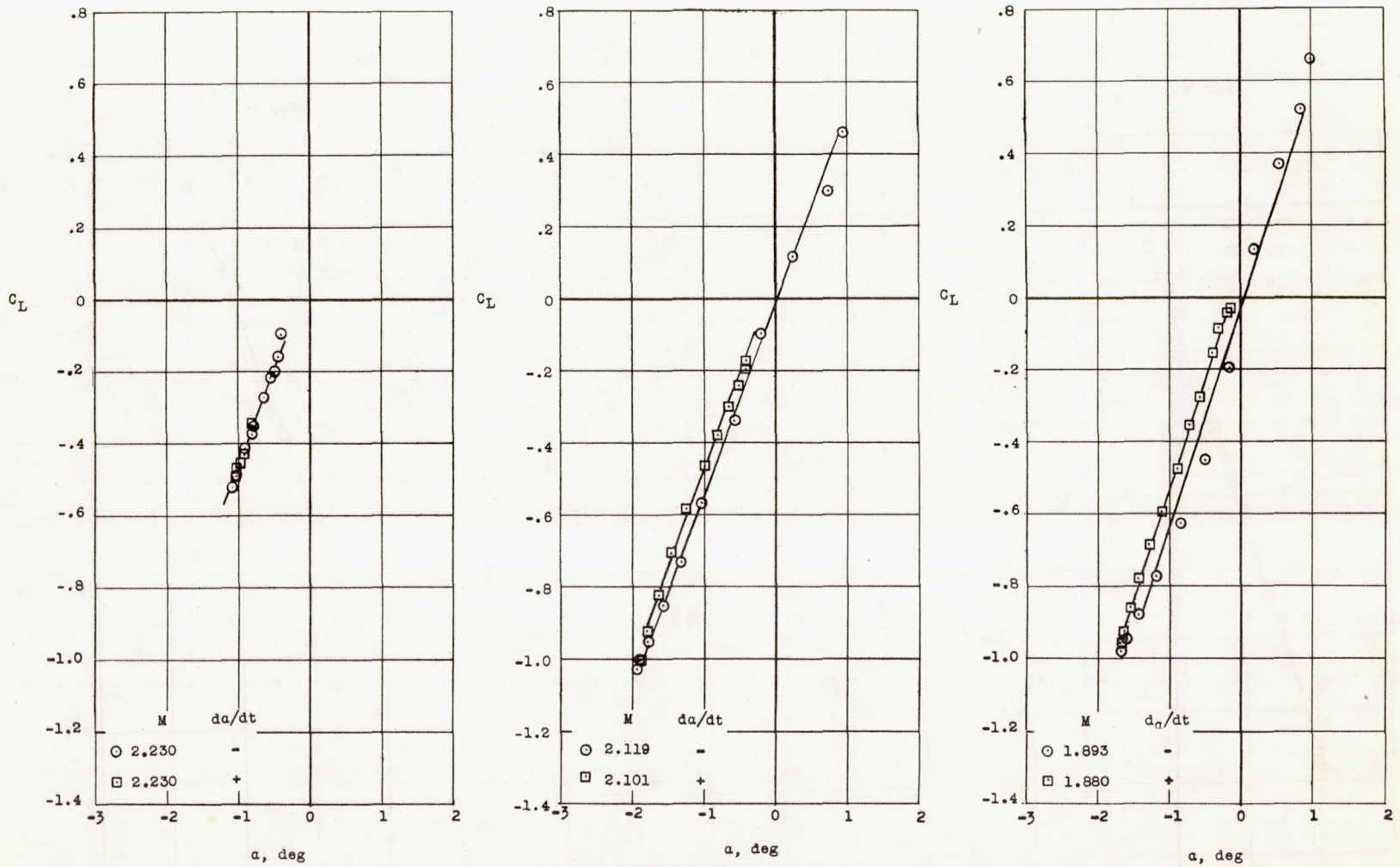


Figure 5.- Variation of Reynolds number, per foot, with Mach number.

CONFIDENTIAL

CONFIDENTIAL

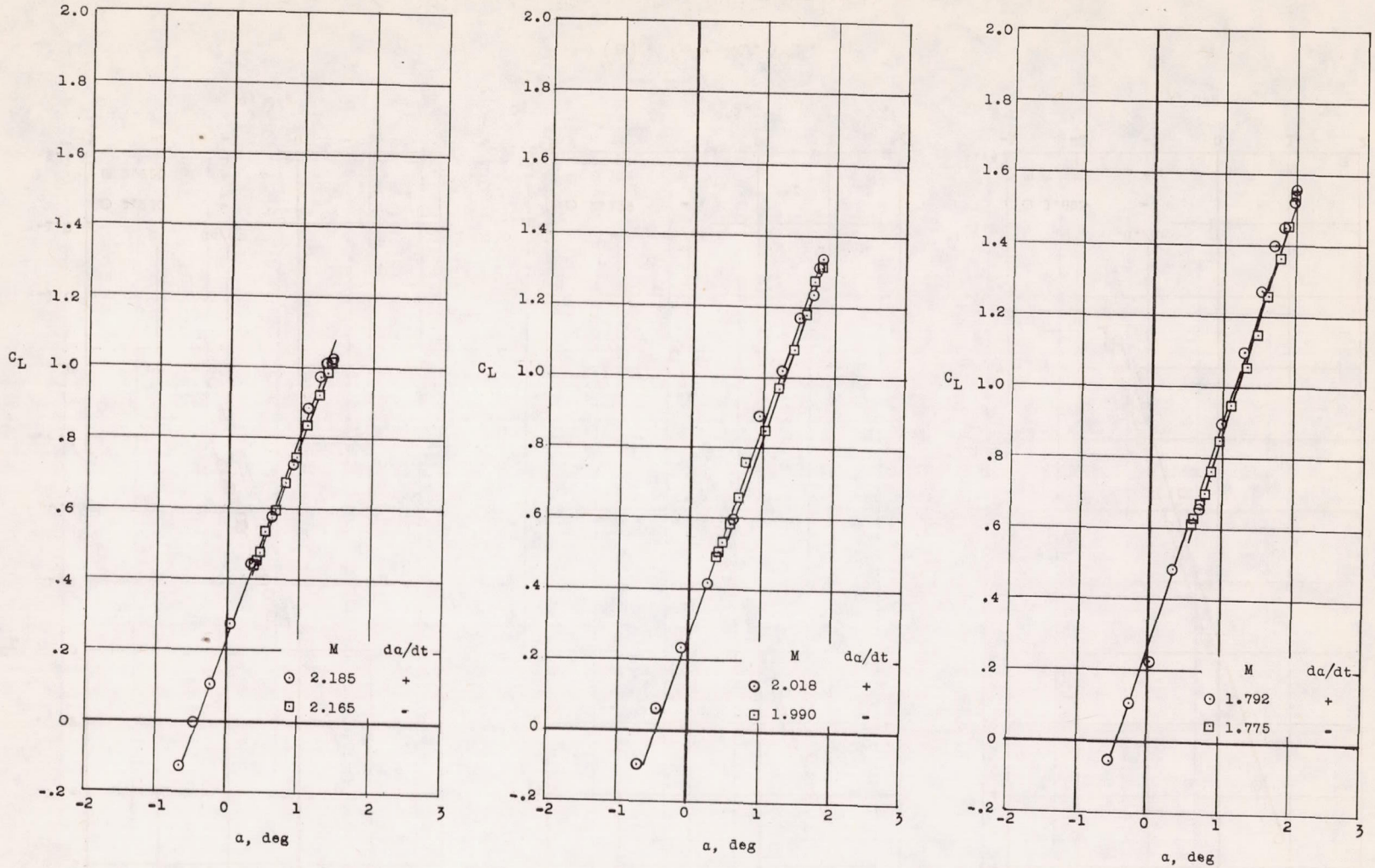


(a) $\delta \approx -0.3°$.

Figure 6.- Variation of lift coefficient with angle of attack.

CONFIDENTIAL

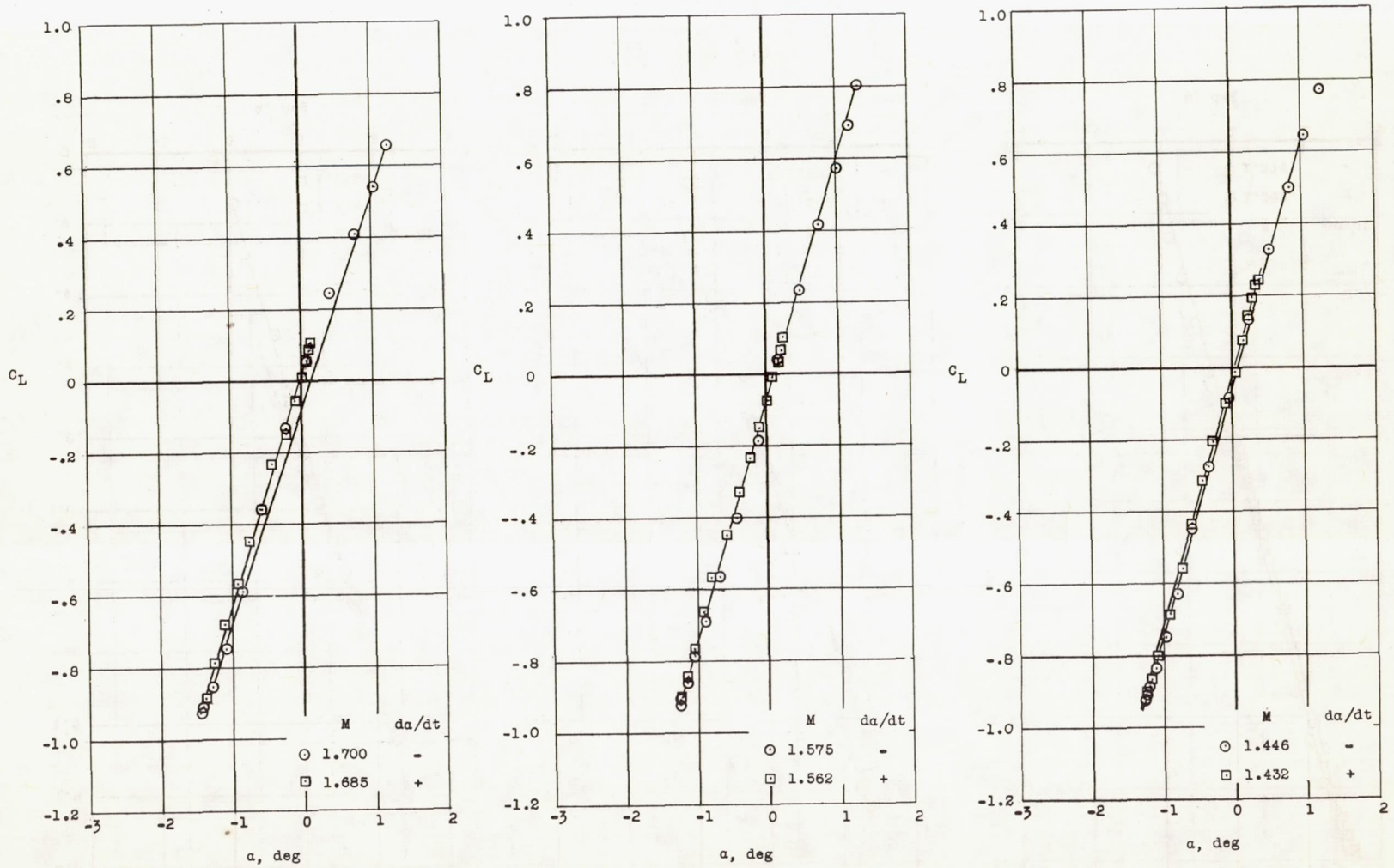
CONFIDENTIAL



(b) $\delta \approx 3.0^{\circ}$.

Figure 6.- Continued.

CONFIDENTIAL

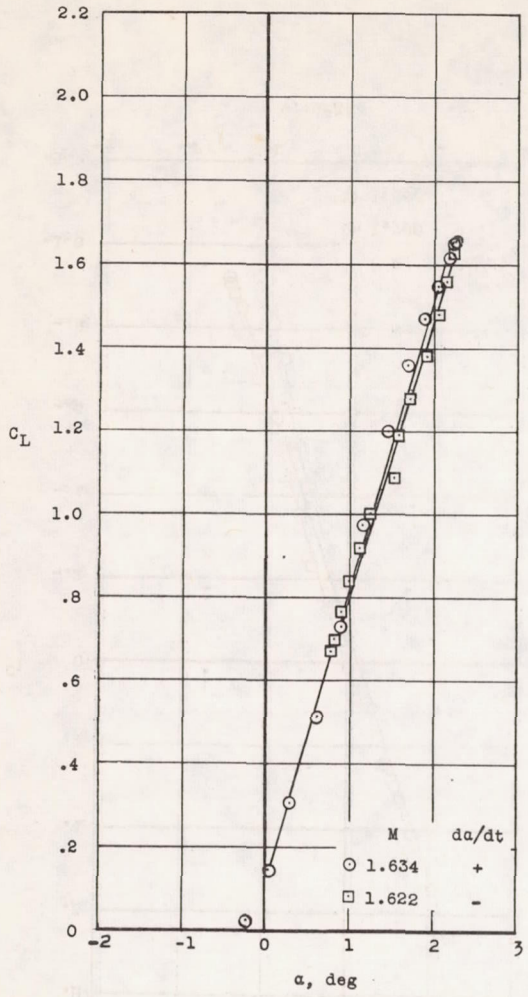


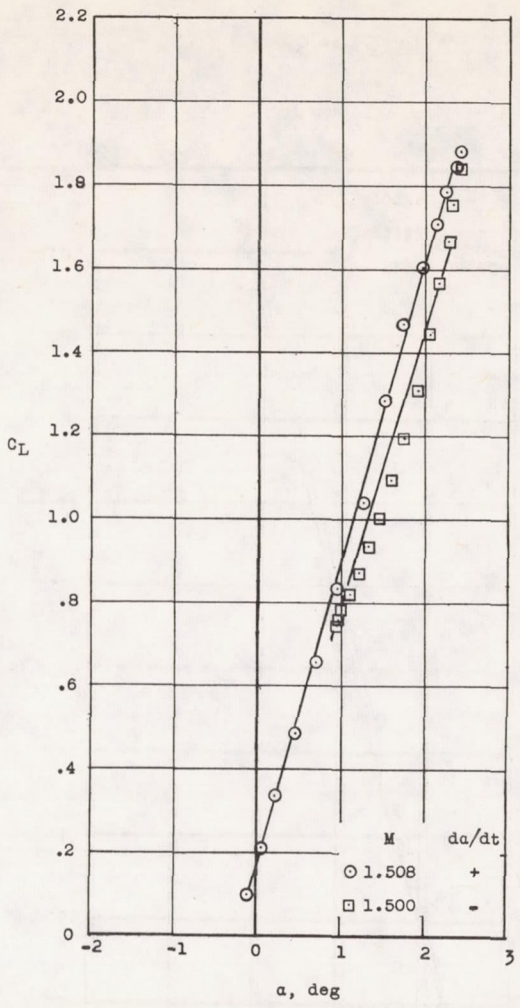
(c) $\delta \approx -0.3^\circ$.

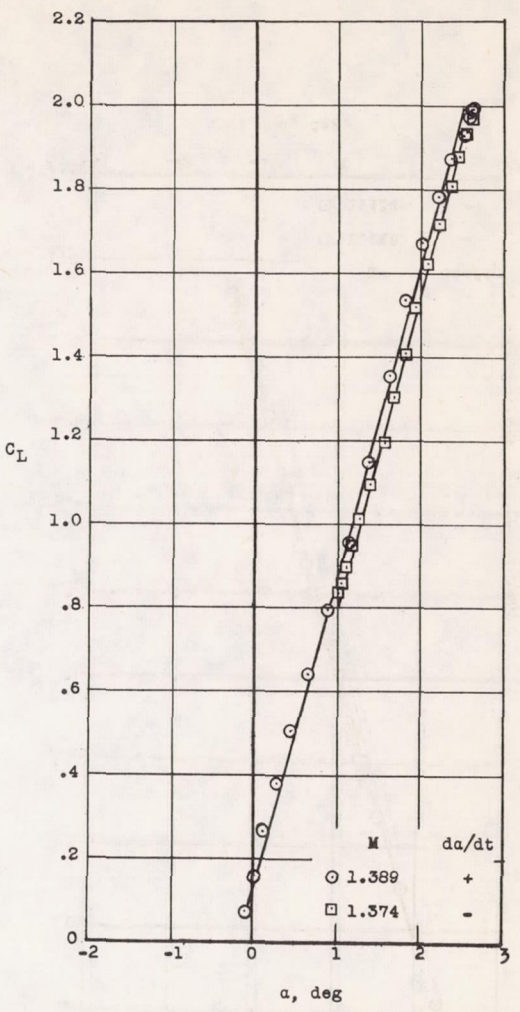
Figure 6.- Continued.

CONFIDENTIAL

CONFIDENTIAL





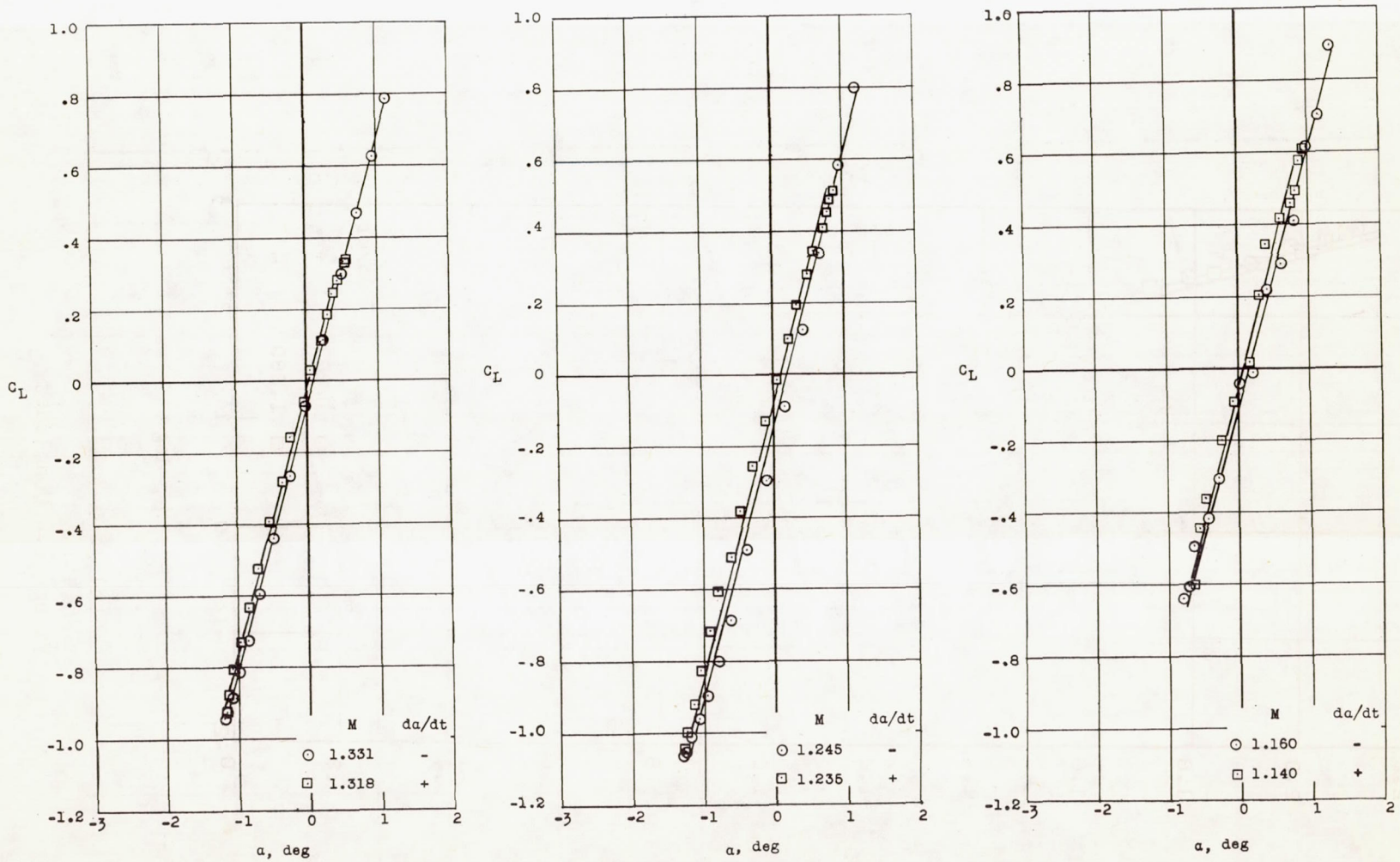


(d) $\delta \approx 3.0^{\circ}$.

Figure 6.- Continued.

CONFIDENTIAL

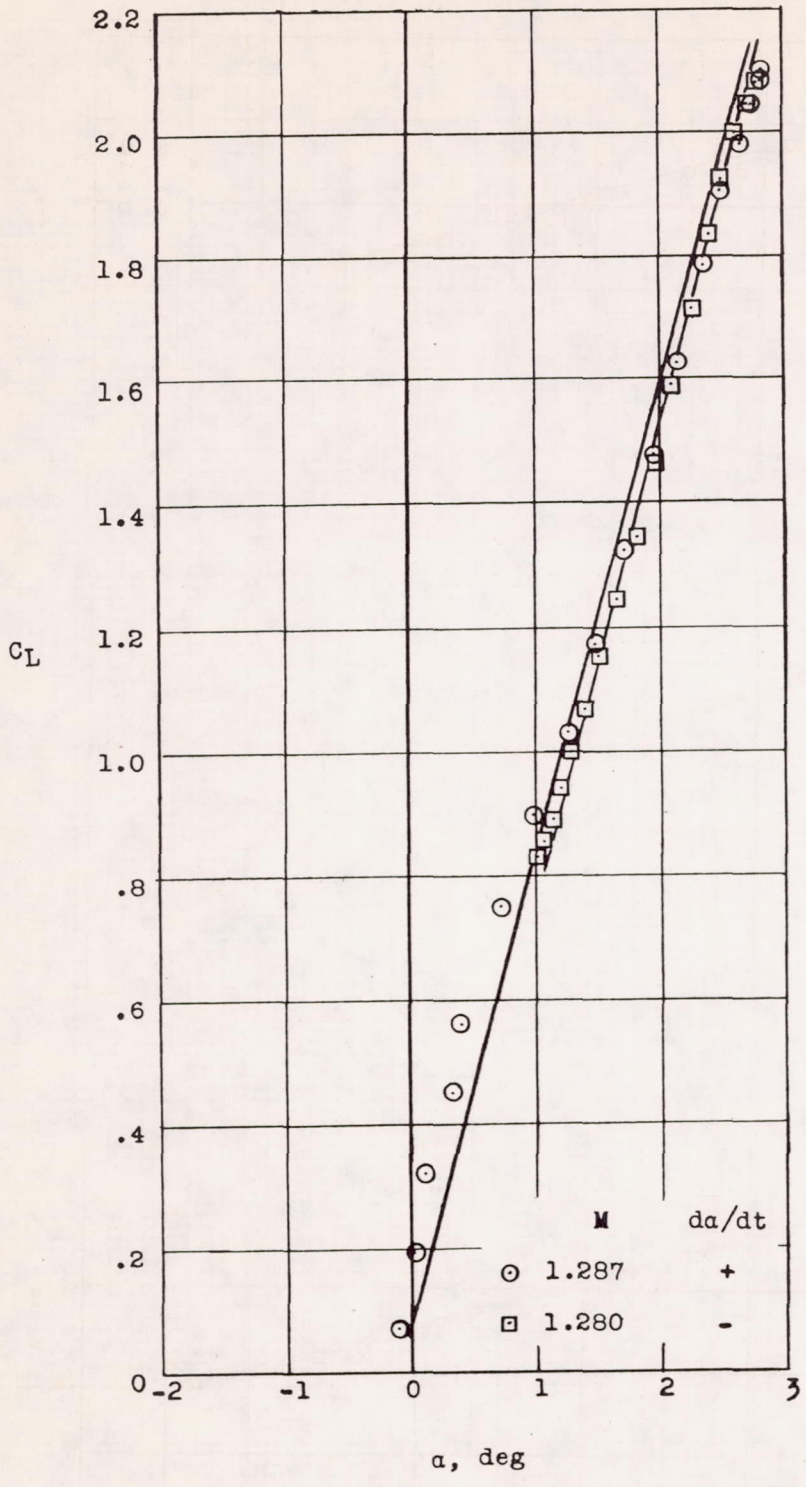
CONFIDENTIAL



(e) $\delta \approx -0.3^\circ$.

Figure 6.- Continued.

CONFIDENTIAL



(f) $\delta \approx 3.0^\circ$.

Figure 6.- Concluded.

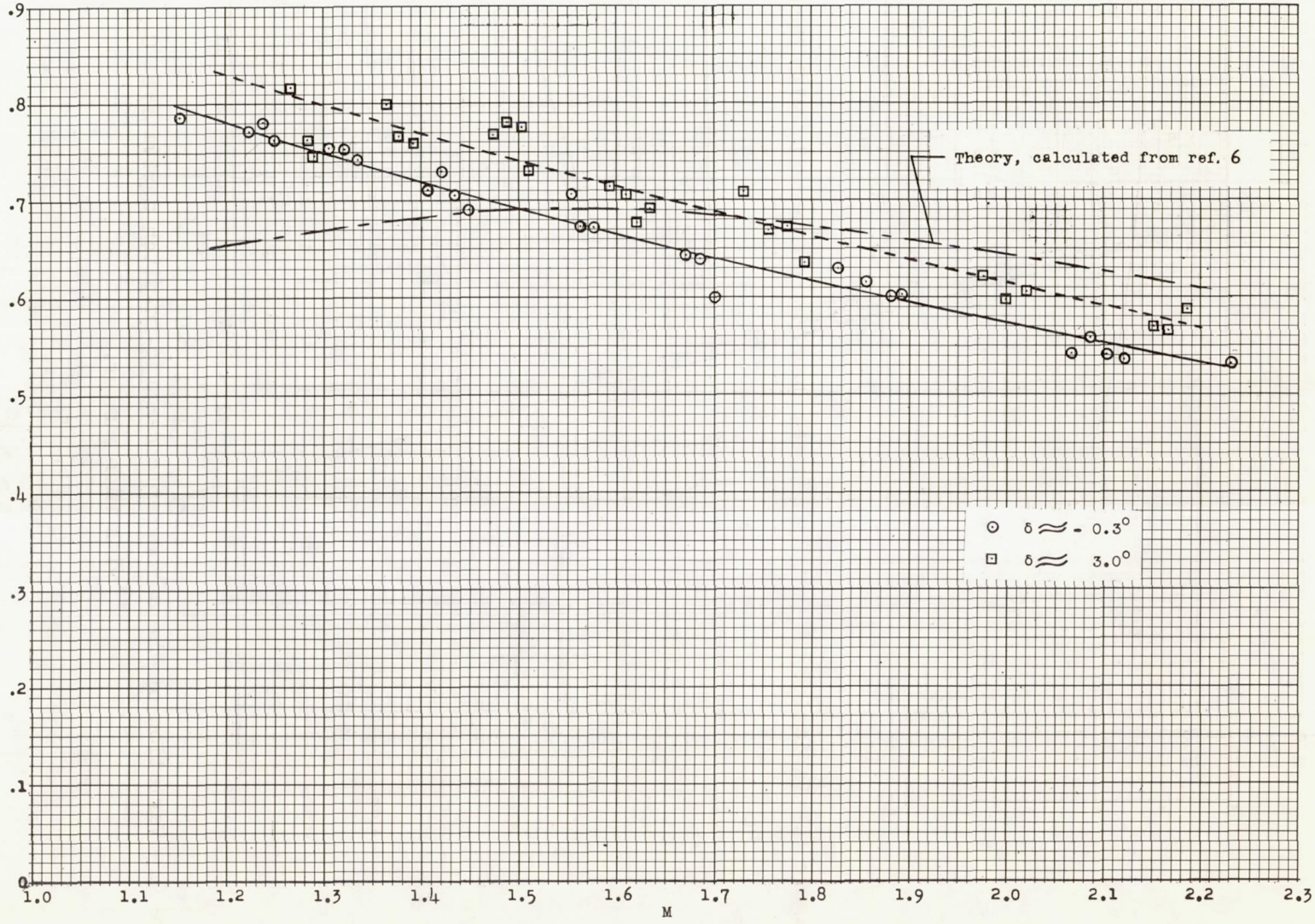


Figure 7.- Variation of average lift-curve slope with Mach number.

CONFIDENTIAL

CONFIDENTIAL

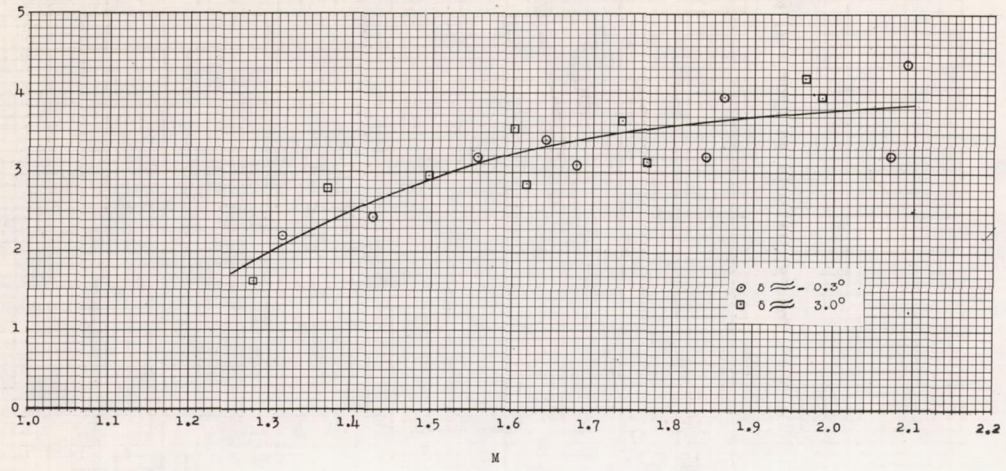


Figure 8.- Variation of the exponential damping constant b with Mach number

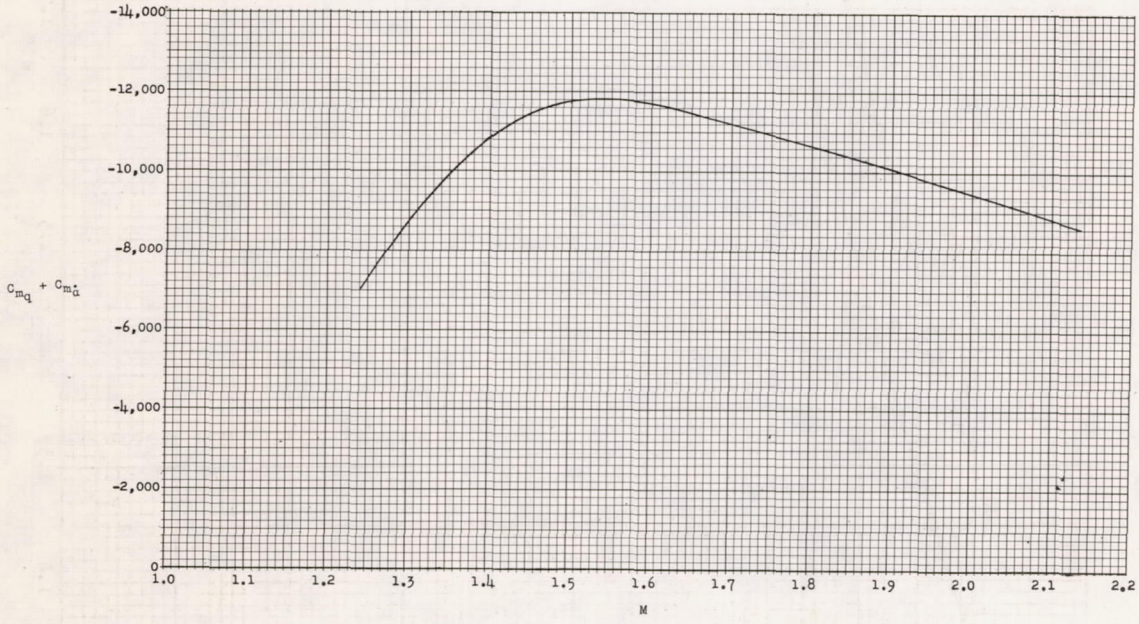


Figure 9.- Variation of the aerodynamic damping-in-pitch derivative $C_{m_q} + C_{m_{\dot{\alpha}}}$ with Mach number.

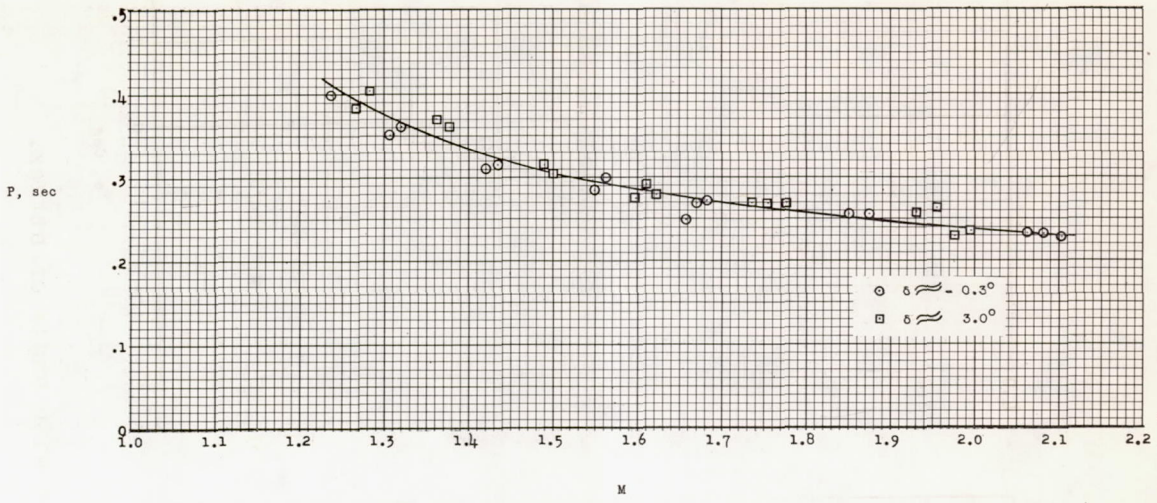


Figure 10.- Variation of period of oscillation with Mach number.

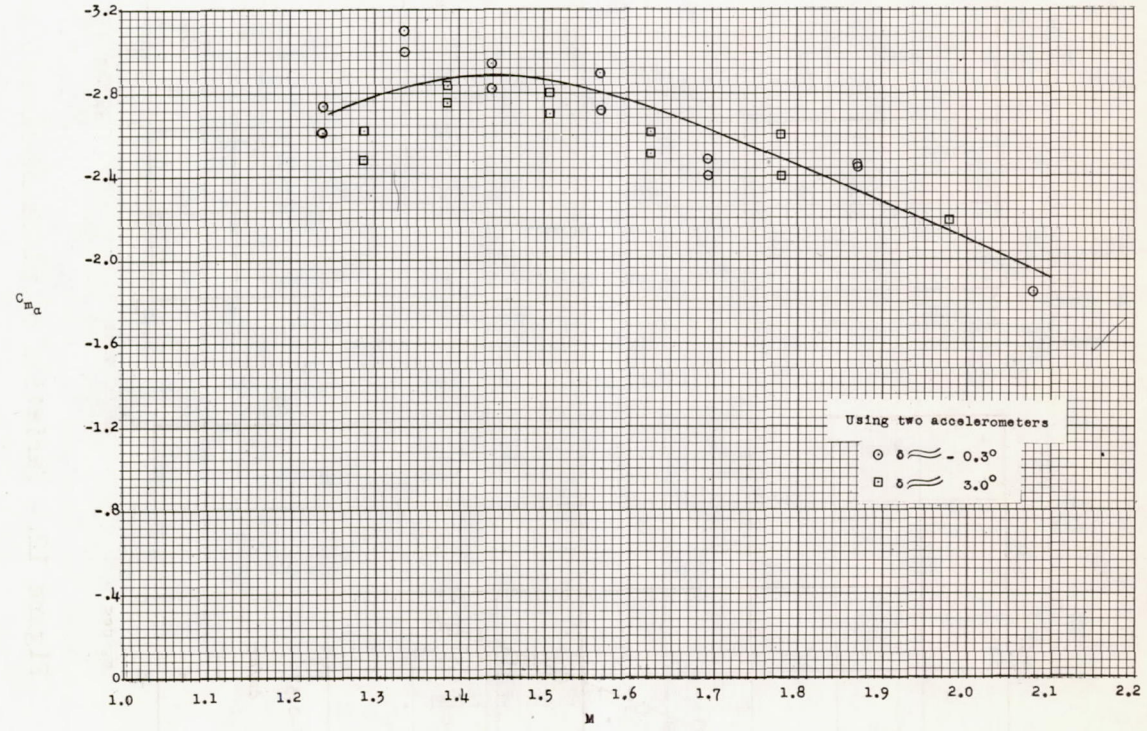


Figure 11.- Variation of the static stability derivative C_{m_α} with Mach number.

CONFIDENTIAL

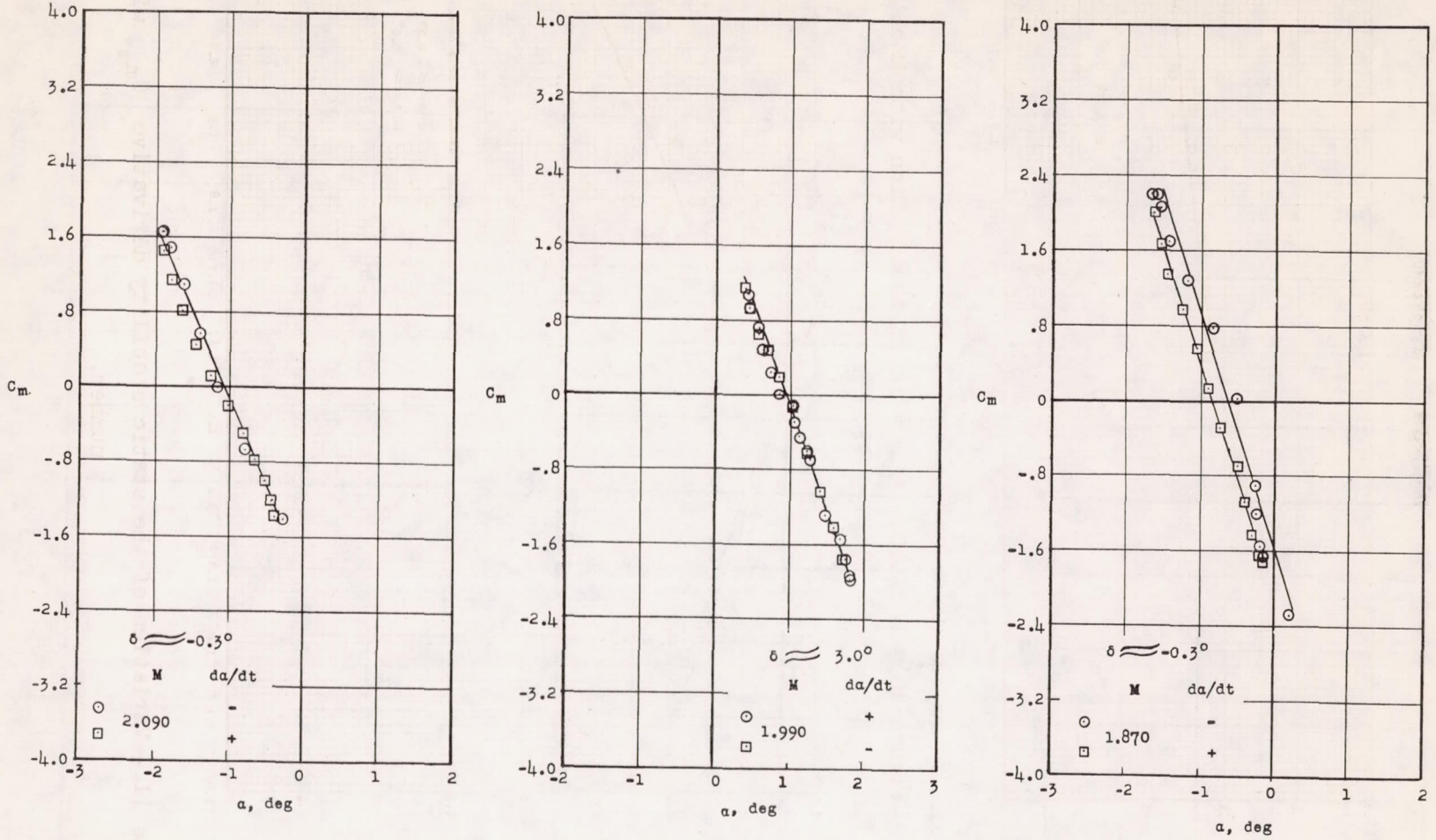


Figure 12.- Variation of pitching-moment coefficient with angle of attack.

CONFIDENTIAL

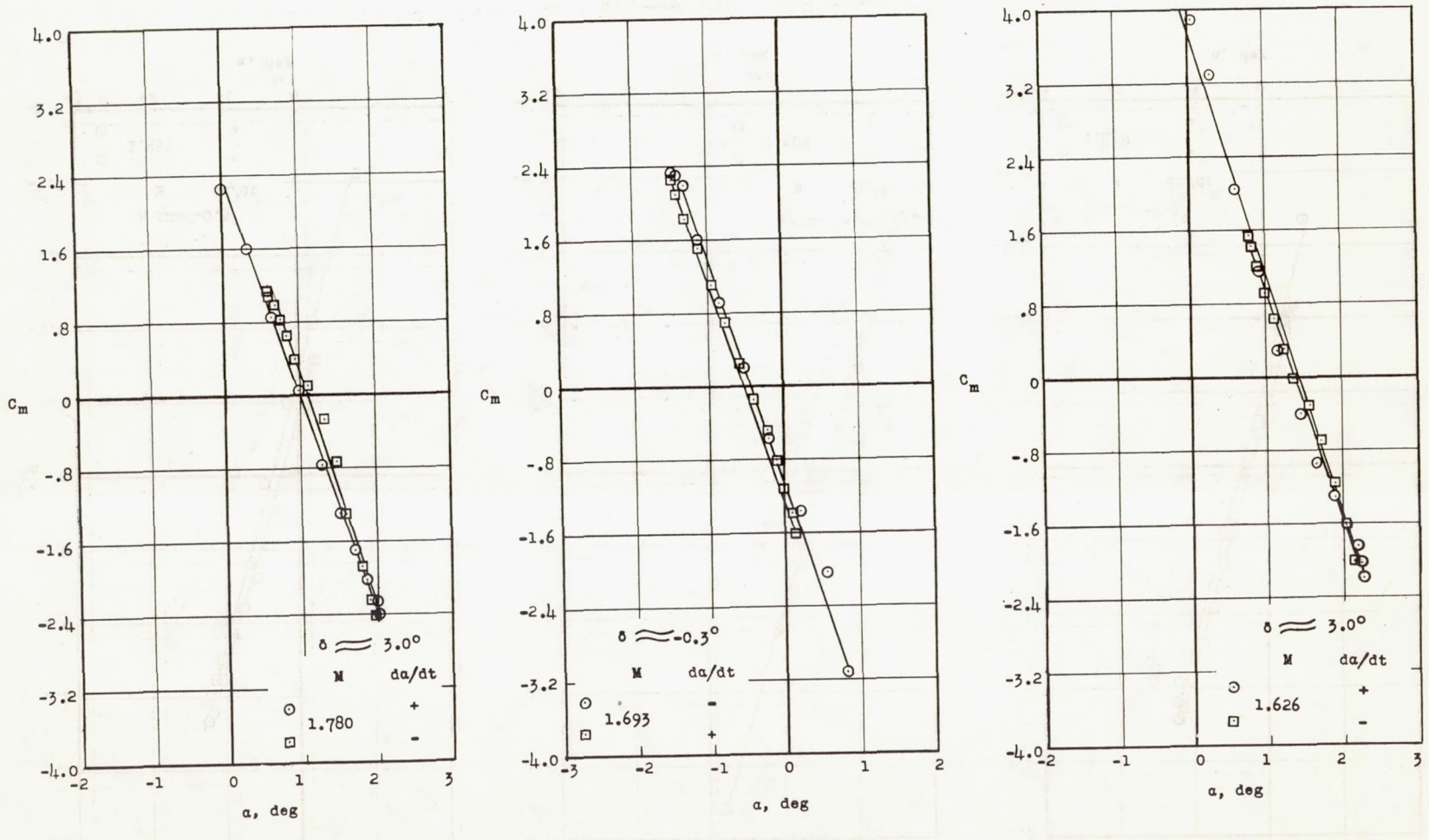
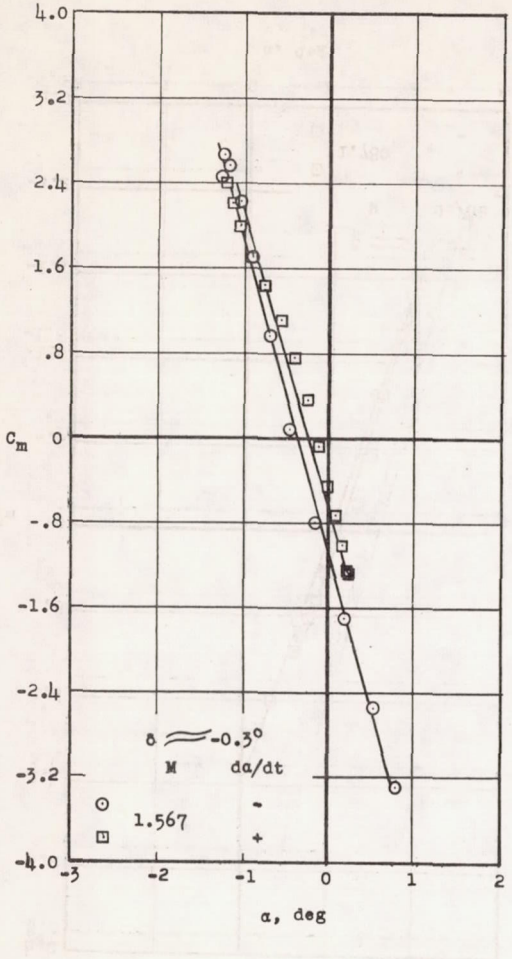
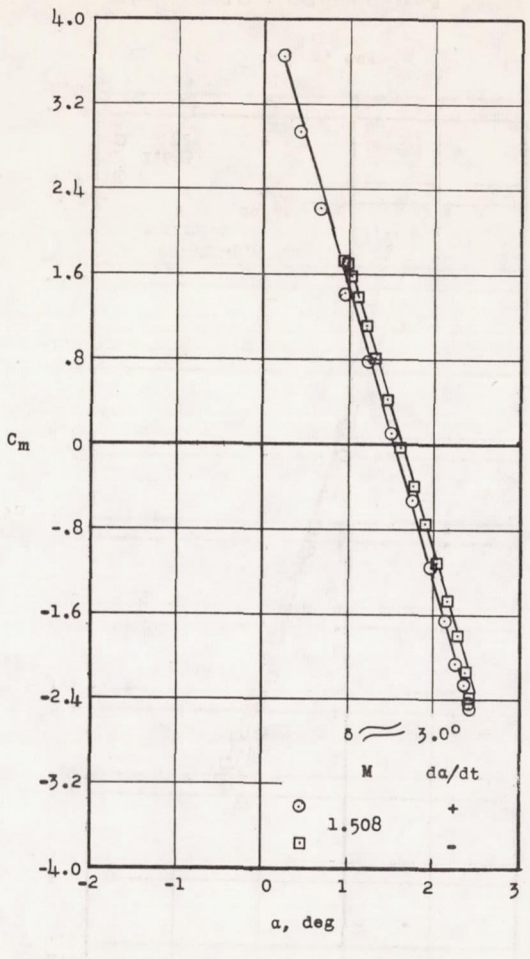


Figure 12.- Continued.

CONFIDENTIAL

CONFIDENTIAL





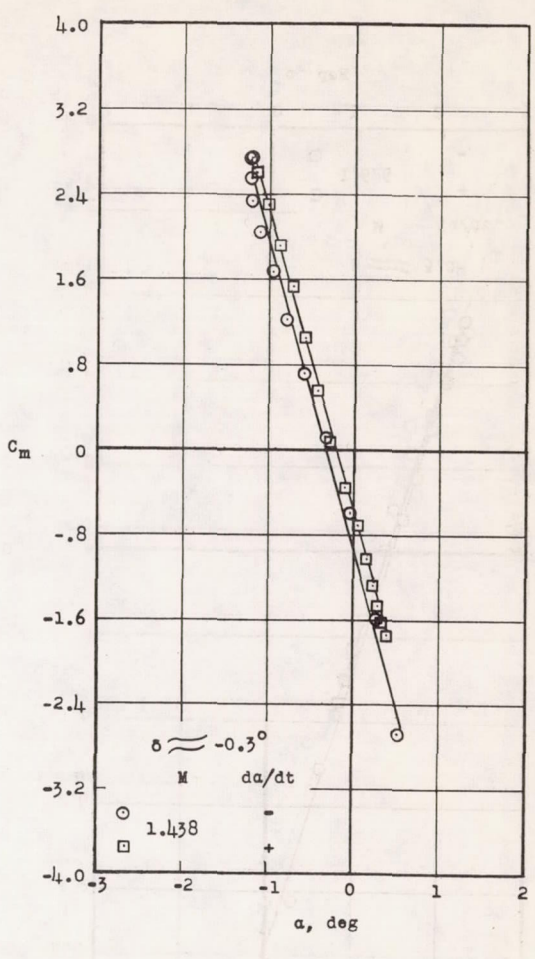


Figure 12.- Continued.

CONFIDENTIAL

CONFIDENTIAL

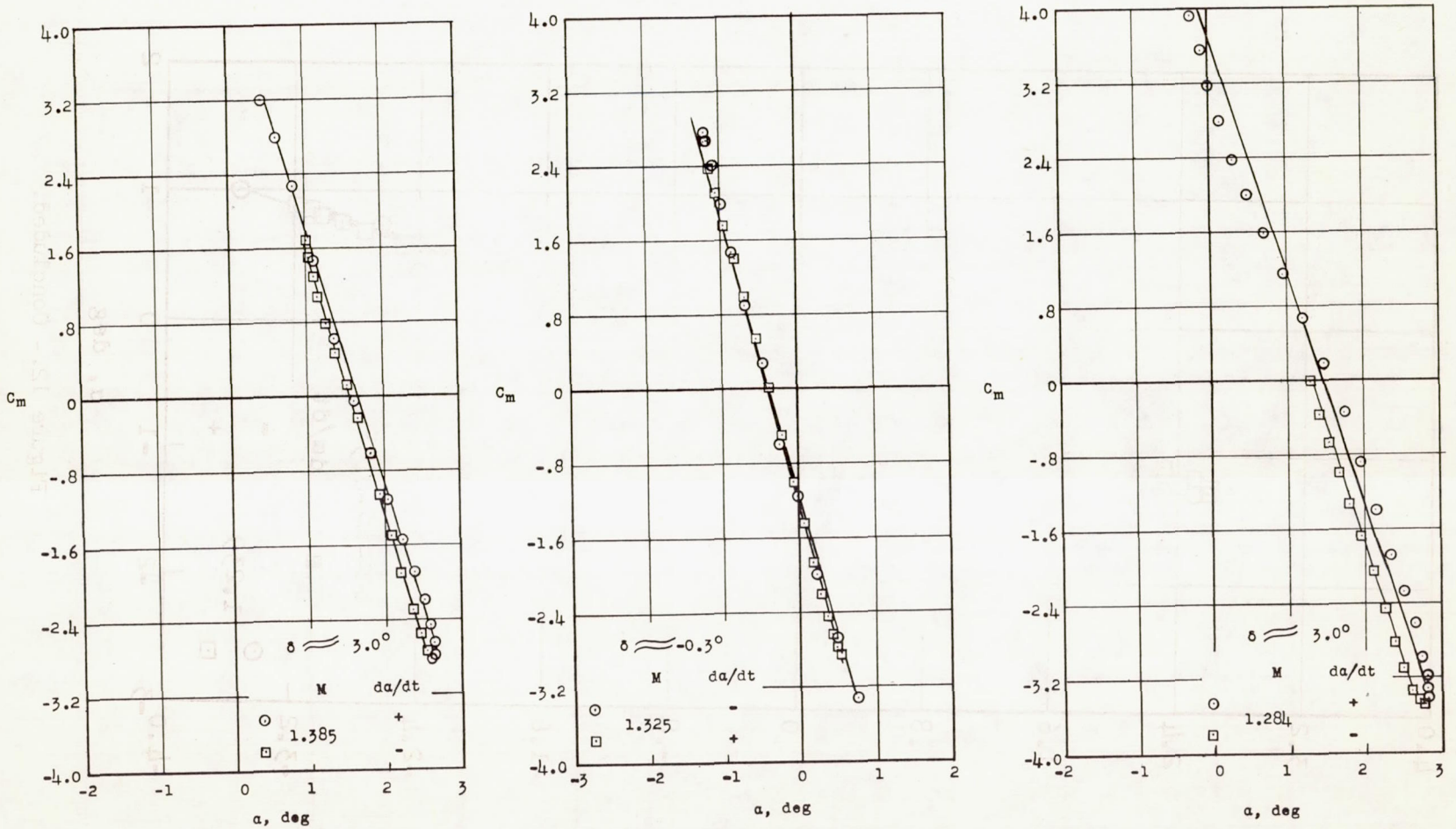


Figure 12.- Continued.

CONFIDENTIAL

DECLASSIFIED

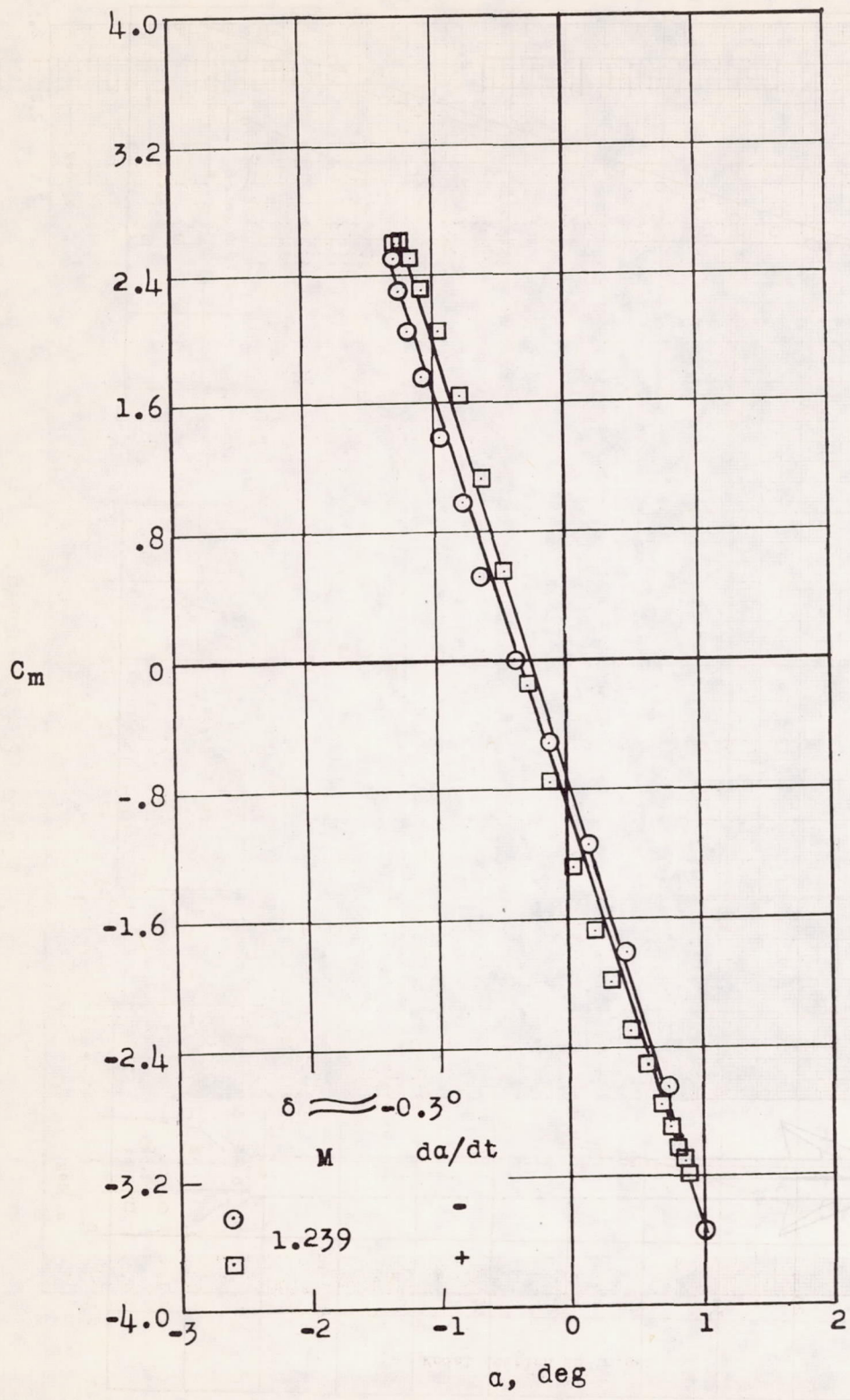


Figure 12.- Concluded.

CONFIDENTIAL

CONFIDENTIAL

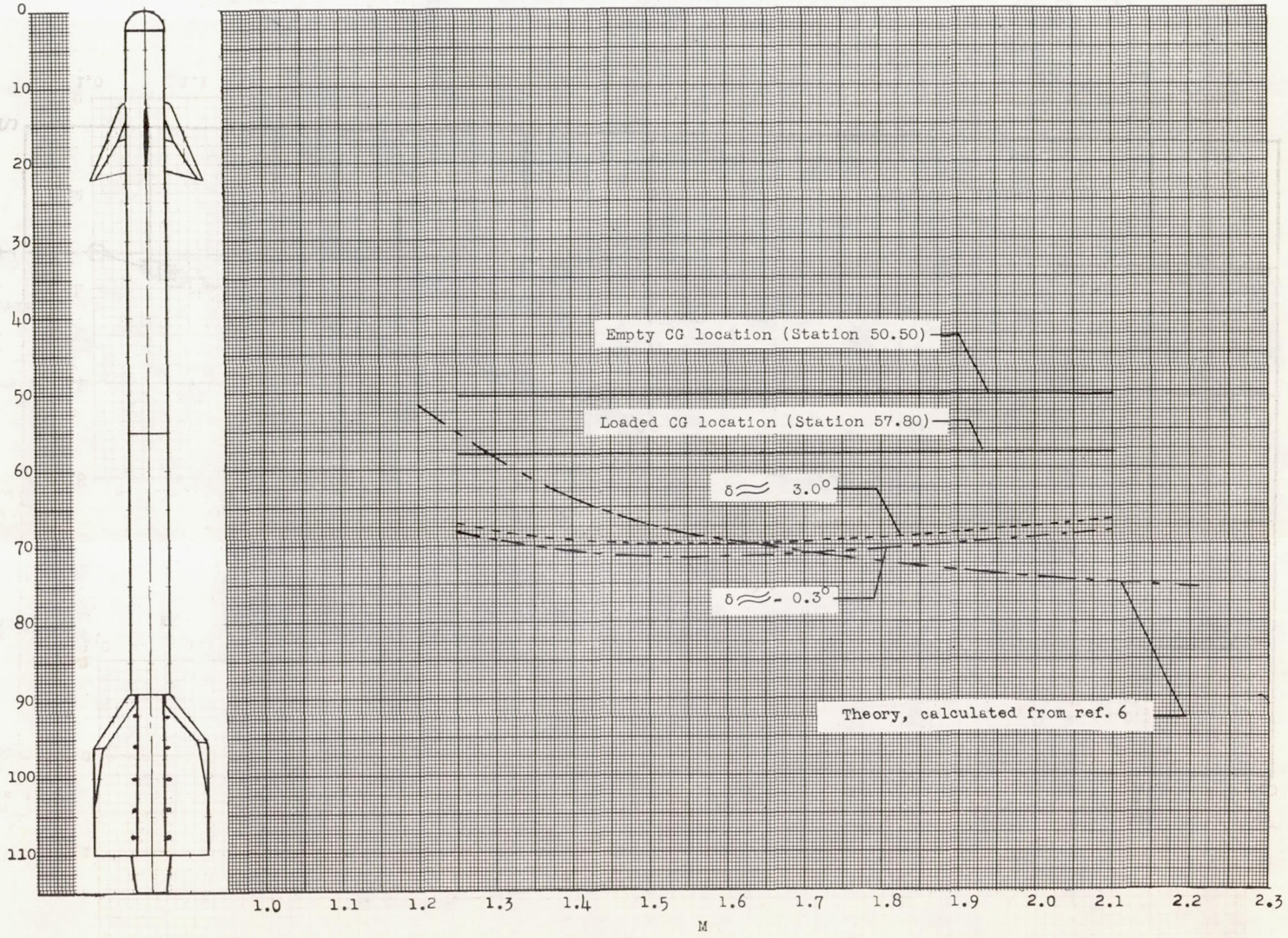


Figure 13.- Variation of the aerodynamic-center location with Mach number.

CONFIDENTIAL

CONFIDENTIAL

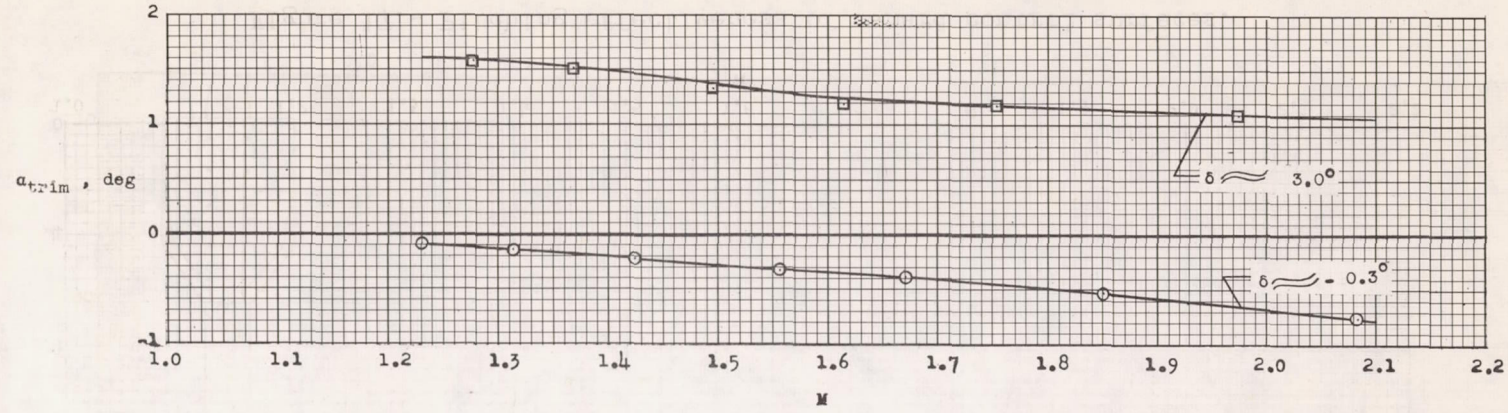


Figure 14.- Variation of trim angle of attack with Mach number.

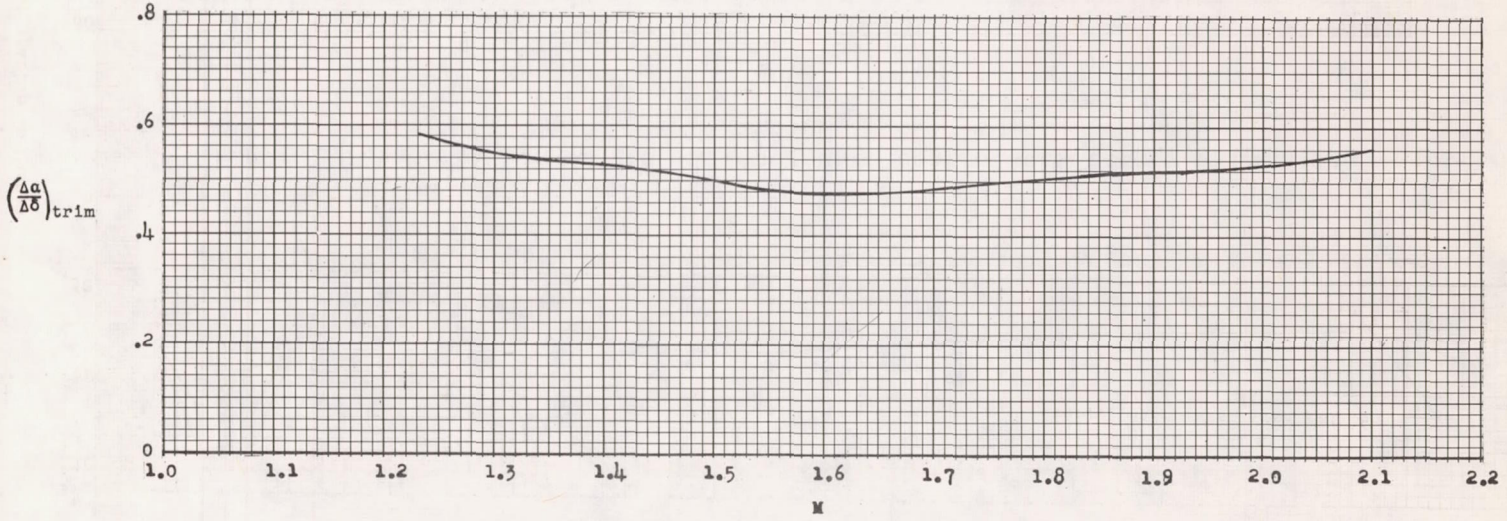


Figure 15.- Variation of the trim angle of attack produced by a unit control deflection with Mach number.

CONFIDENTIAL

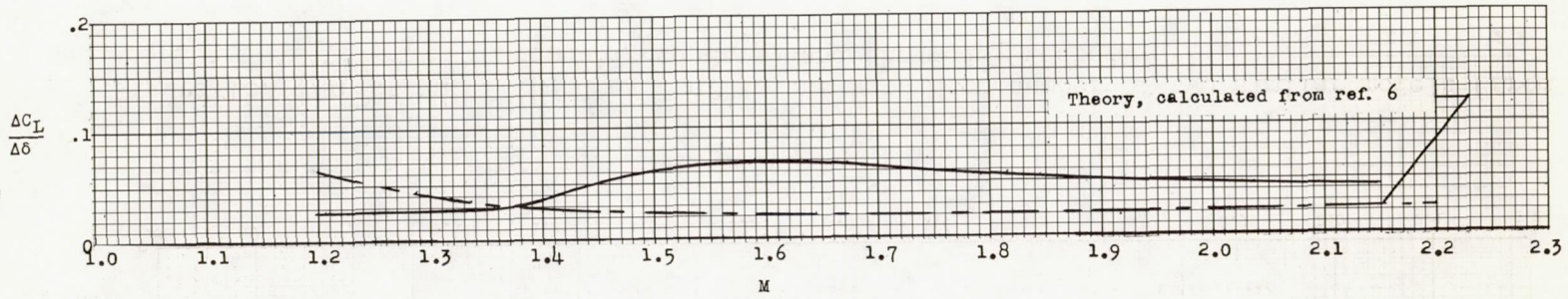


Figure 16.- Variation of the lift per unit control deflection with Mach number.

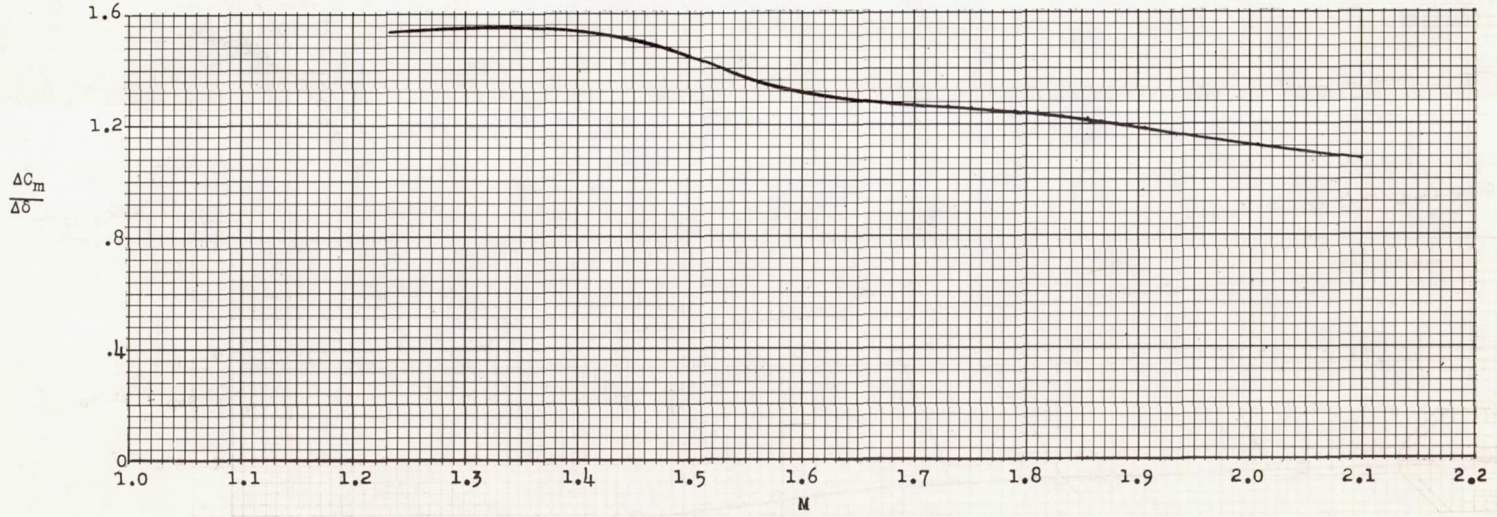


Figure 17.- Pitching effectiveness of canard control surfaces.

CONFIDENTIAL

CONFIDENTIAL

CONFIDENTIAL

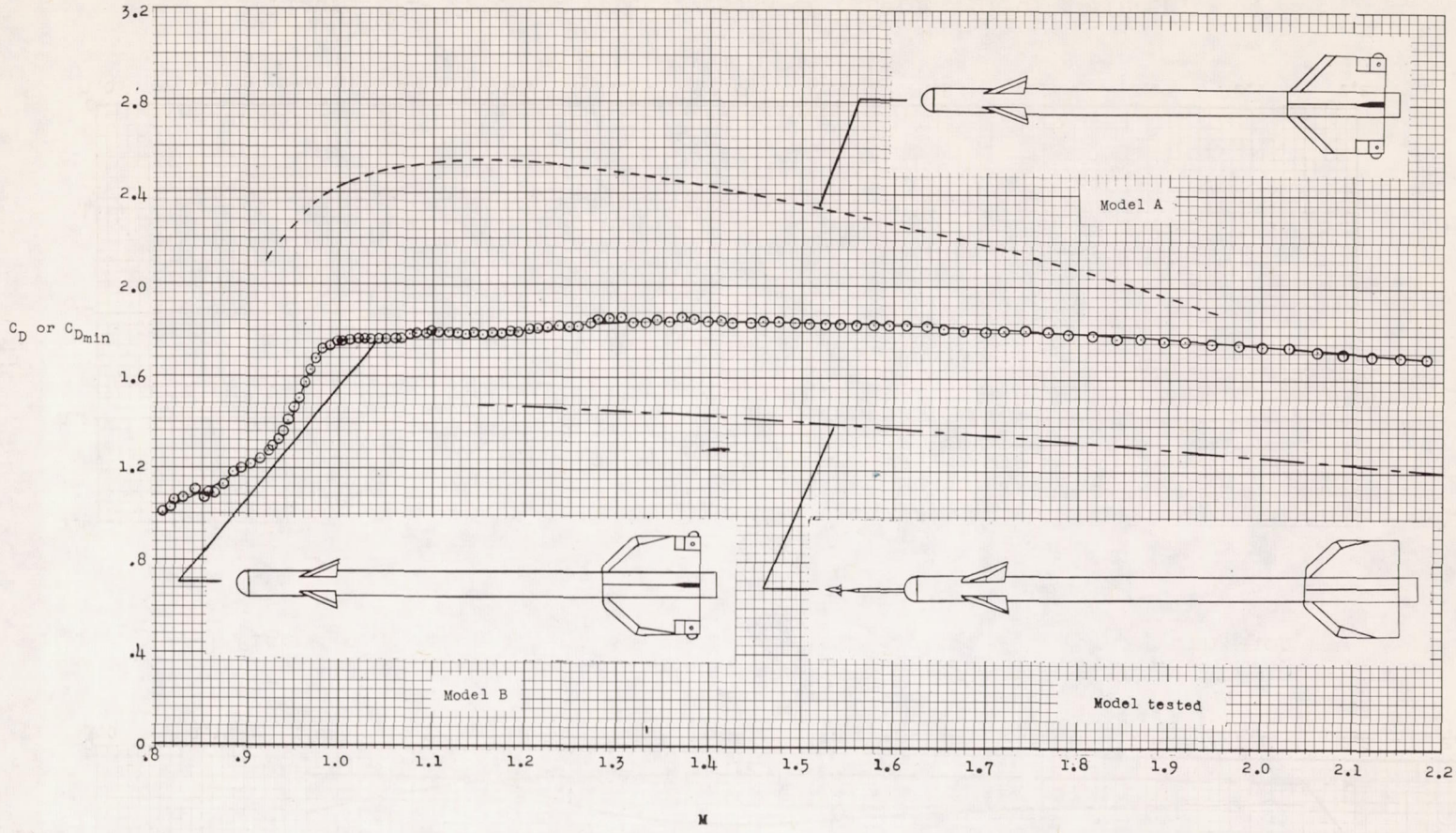


Figure 18.- Variation of the drag coefficient with Mach number of two similar models (from unpublished data) and the model tested.

NACA - Langley Field, Va.

CONFIDENTIAL

CONFIDENTIAL

CONFIDENTIAL